Available online at www.sciencedirect.com
SCIENCE DIRECT®
Journal of Sound and Vibration 291 (2006) 132–168
JOURNAL OF SOUND AND VIBRATION
www.elsevier.com/locate/jsvi

Stick and non-stick periodic motions in periodically forced oscillators with dry friction

Albert C.J. Luo*, Brandon C. Gegg

Department of Mechanical and Industrial Engineering, Southern Illinois University Edwardsville, Edwardsville, IL 62026-1805, USA

Received 28 September 2004; received in revised form 10 May 2005; accepted 1 June 2005
Available online 22 August 2005

Abstract

In this paper, the force criteria for stick and non-stick motions in harmonically forced, friction-induced oscillators are developed from the local theory of non-smooth dynamical systems on connectable domains. The periodically driven, linear oscillator with a simple dry friction is considered as a sampled problem to demonstrate the methodology presented in this paper. With appropriate mapping structures, the force criteria give the analytical predictions of the stick and non-stick, periodic motions for such an oscillator. Furthermore, the effects of external excitations and friction forces on the stick and non-stick motions are discussed, and the corresponding regions of specified motions in parameter space are obtained. The sliding and grazing phenomena for this oscillator are also presented in this paper. However, an extensive investigation on sliding and grazing bifurcations should be carried out in sequel. The displacement, velocity and force responses for stick and non-stick, periodic motions are illustrated for a better understanding of the dynamics mechanism of stick and non-stick motions of the dry-friction oscillator. The force criteria and mapping techniques are also applicable to multi-body contact dynamics. The methodology presented in this paper can be applied for numerical predictions of motions in nonlinear, non-smooth dynamical systems.

*Corresponding author. Tel.: +1 618 650 5389; fax: +1 618 650 2555.
E-mail address: aluo@siue.edu (A.C.J. Luo).

0022-460X/$ - see front matter © 2005 Elsevier Ltd. All rights reserved.
doi:10.1016/j.jsv.2005.06.003

1. Introduction

Friction-induced oscillations extensively exist in engineering, such as disk brake systems, turbine blades and string music instruments. The discontinuity of the system, caused by friction forces, makes this oscillation problem difficult to solve theoretically and numerically. Therefore, the friction-induced oscillations have been of great interest for a long time. An idealized mechanical model for the friction-induced oscillator is introduced in this paper through the simplest mechanical problem. Consider a periodically forced oscillator consisting of a mass (m), a spring of stiffness (k) and a damper of viscous damping coefficient (r), as shown in Fig. 1(a). This oscillator slides or rests on the horizontal belt surface traveling with a constant speed (V). The absolute coordinate system (x,t) is for the mass. Consider a periodical force $Q_0 \cos \Omega t$ exerting on the mass, where Q_0 and Ω are the excitation strength and frequency, respectively. Since the mass contacts the moving belt with friction, the mass can move along, or rest on, the belt surface. Further, a kinetic friction force shown in Fig. 1(b) is described as

$$\bar{F}_f(\dot{x}) \begin{cases} = \mu_k F_N, & \dot{x} \in [V, \infty), \\ \in \left[-\mu_k F_N, \mu_k F_N\right], & \dot{x} = V, \\ = -\mu_k F_N, & \dot{x} \in (-\infty, V], \end{cases} \tag{1}$$

where $\dot{x} \triangleq \mathrm{d}x/\mathrm{d}t$, μ_k, and F_N are a friction coefficient and a normal force to the contact surface, respectively. For the model in Fig. 1, the friction force is $F_N = mg$ where g is the gravitational acceleration.

For the mass moving with the same speed of the belt surface, the non-friction forces acting on the mass in the x-direction is defined as

$$F_s = A_0 \cos \Omega t - 2dV - cx \quad \text{for } \dot{x} = V, \tag{2}$$

where $A_0 = Q_0/m$, $d = r/2m$ and $c = k/m$. This force cannot overcome the friction force for stick motions, i.e., $|F_s| \leqslant |F_f|$ and $F_f = \mu_k F_N/m$. Therefore, the mass does not have any relative motion to the belt. In other words, no acceleration exists, i.e.,

$$\ddot{x} = 0 \quad \text{for } \dot{x} = V. \tag{3}$$

If $|F_s| > |F_f|$, the non-friction force will overcome the static friction force on the mass and the non-stick motion will appear. For the non-stick motion, the total force acting on the mass is

$$F = A_0 \cos \Omega t - F_f \operatorname{sgn}(\dot{x} - V) - 2d\dot{x} - cx \quad \text{for } \dot{x} \neq V; \tag{4}$$

$\operatorname{sgn}(\cdot)$ is the sign function. Therefore, the equation of the non-stick motion for this oscillator with the dry friction is

$$\ddot{x} + 2d\dot{x} + cx = A_0 \cos \Omega t - F_f \operatorname{sgn}(\dot{x} - V) \quad \text{for } \dot{x} \neq V. \tag{5}$$

Based on the above model, Luo and Gegg [1] generalized the mathematical model for friction-induced oscillators. The mechanism of the stick and non-stick motions for such a model was briefly studied to obtain the conditions for the onset and vanishing of stick motion in such a non-smooth dynamical system. The comprehensive investigation of the generalized friction-induced oscillator will be carried out in this paper. Under different parameters, periodic motions in parameter space will be discussed for a better understanding of the dynamics mechanism of the

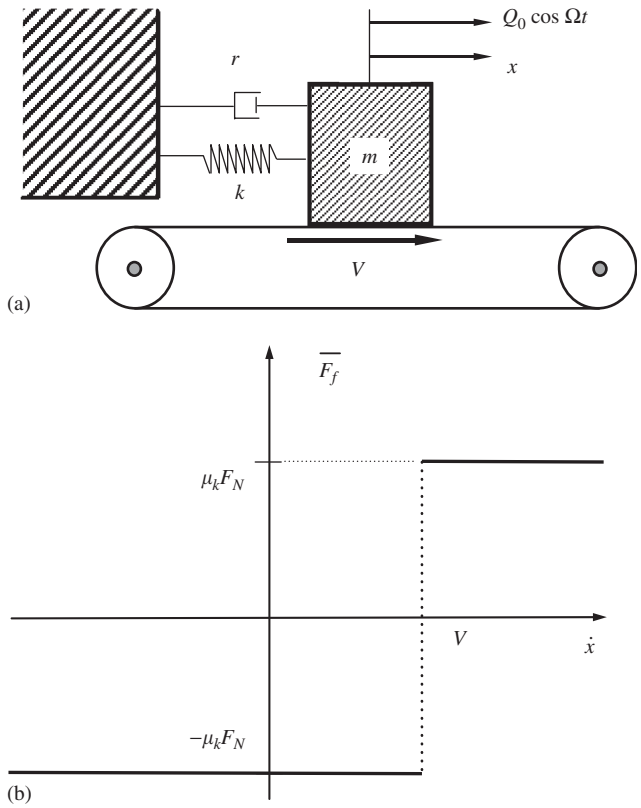

Fig. 1. The mechanical model of a linear oscillator with dry friction: (a) schematic and (b) friction force.

harmonically forced, linear oscillator with dry friction. The regions of specific periodic motions in parameter space will be presented for practical applications in engineering.

Den Hartog [2] initialized an investigation on the periodic motion of the forced linear oscillator with Coulomb and viscous damping in 1930. From mathematical points of views, Levitan [3] discussed a friction oscillation model with the periodically driven base in 1960, and the stability of the periodic motion was presented. In 1979, Hundal [4] further discussed the dynamical responses of the base driven friction oscillator. In 1986 Shaw [5] investigated the stability for such a non-stick, periodic motion through the Poincare mapping. In 1992, Feeny [6] investigated the non-smoothness of the Coulomb friction oscillator and presented the stick region analytically and graphically. In 1994, Feeny and Moon [7] did the experimental and numerical investigations of chaos in a dry-friction oscillator. In 1996 Feeny [8] gave the systematical investigation of the nonlinear dynamics of oscillators with stick–slip friction. In 1997 Hinrichs et al. [9] investigated the dynamics of oscillator with impact and friction (also see Ref. [10]). The stick and non-stick motions were observed, and chaos for a nonlinear friction model was presented. In 1998, Natsiavas [11] investigated the stability of piecewise linear oscillators with viscous and dry friction damping through the perturbation of the initial conditions (also see Ref. [12]). Leine et al. [13] determined the limit cycles of the nonlinear friction model by the shooting method. In 1999, Virgin and Begley [14] used the interpolated cell mapping method to obtain the grazing

bifurcation and attraction basin of an impact-friction oscillator. In addition, the approximate solutions of responses in friction-induced oscillation were of great interest in recent years. In 2001, Ko et al. [15] investigated the fiction-induced vibrations with and without external excitations. In 2002, Andreaus and Casini [16] achieved the closed-form solutions of the Coulomb friction-impact model without external excitations. The approximate, analytical amplitude for stick–slip vibration with nonlinear friction model was presented by Thomsen and Fidlin [17] in 2003. Kim and Perkins [18] used the harmonic balance/Galerkin method to investigate non-smooth stick–slip oscillator. In 2004, Pilipchuk and Tan [19] investigated the friction-induced vibration of a two-degree-of-freedom (2dof) mass–damper–spring system interacting with a decelerating rigid strip.

In 1995, Luo [20] initialized the mapping structure concept to determine the periodic motion for impact oscillators (also see, Refs. [21,22]). This methodology was used to investigate the periodic and chaotic motions of the periodically driven piecewise linear systems in Refs. [23,24]. A generalized methodology for complex periodic motions was given through investigation of such a piecewise linear system [25]. In 1994, Pfeiffer [26] considered the impacts and frictions to investigate the unsteady process in machines. To further investigate the non-smooth dynamical systems, in 1996 Glocker and Pfeiffer [27] developed the theory for multi-body dynamics with unilateral contacts by using analytical dynamics. In 1999, Pfeiffer [28] gave a brief survey of the theory of the unilateral multi-body dynamics, and presented some typical applications (also see Ref. [29]). From mathematical points of view, in 1964, Filippov [30] presented differential equations with discontinuous right-hand sides, which started from the Coulomb friction oscillator. The concept of differential inclusion was introduced via the set-valued analysis, and the existence and uniqueness of the solution for such a discontinuous differential equation were discussed. The comprehensive discussion of such discontinuous differential equations can be referred to Ref. [31]. However, Filippov's theory mainly focused on the existence and uniqueness of the solutions for non-smooth dynamical systems. The local singularity caused by the separation boundary was not discussed. In order to analyze the complexity of non-smooth dynamical systems, in 2005, Luo [32] developed a general theory for the local singularity of non-smooth dynamical systems on connectable domains. The local singularity of non-smooth dynamical systems near the separation boundary was discussed. The imaginary, sink and source flows were introduced in Ref. [33] to determine the sliding and source motions in non-smooth dynamical systems.

In this paper, the force criteria for stick and non-stick motions in a forced linear oscillator with dry friction will be developed. The mapping structures of periodic motions in such an oscillator will be constructed. The parameter studies for stick and non-stick, periodic motions will be completed by use of the force criteria. The displacement, velocity and force responses of the stick and non-stick, periodic motions will be simulated for a better understanding of the dynamics mechanism of stick and non-stick motions.

2. Basic theory

A brief introduction to non-smooth dynamical systems in Refs. [32,33] is presented to investigate the dynamics mechanism of stick and non-stick motions. Consider a planar, dynamic system consisting of n-dynamic sub-systems in a universal domain $\overline{\Omega} \subset \Re^2$, divided into n

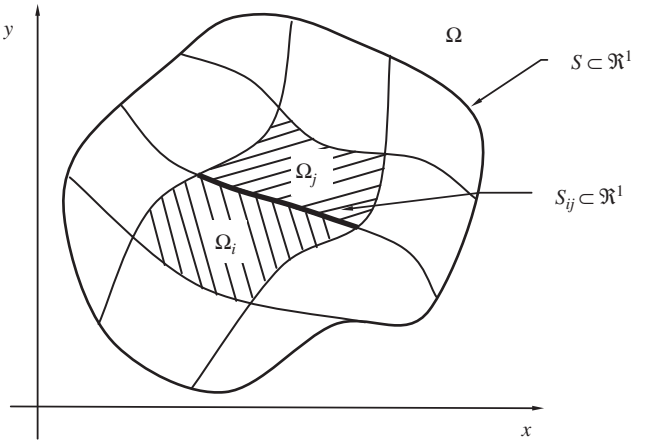

Fig. 2. Connectable sub-domains in phase space

accessible sub-domains Ω_i; and the union of all the accessible sub-domains $\bigcup_{i=1}^{n}\Omega_i$, as shown in Fig. 2. On the ith sub-domain, there is a continuous system in form of

$$\dot{\mathbf{x}} \equiv \mathbf{F}^{(i)}\left(\mathbf{x}, t, \boldsymbol{\mu}_i, \boldsymbol{\pi}\right) = \mathbf{f}^{(i)}\left(\mathbf{x}, \boldsymbol{\mu}_i\right) + \mathbf{g}(\mathbf{x}, t, \boldsymbol{\pi}), \quad \mathbf{x} = (x, y)^{\mathrm{T}} \in \Omega_i, \tag{6}$$

where $\mathbf{g} = (g_1, g_2)^{\mathrm{T}}$ is a bounded, periodic vector function with period T and a parameter vector $\boldsymbol{\pi} = (\pi_1, \pi_2, \ldots, \pi_m)^{\mathrm{T}} \in \Re^m$. Note that the superscript "T" represents the transpose. The vector field $\mathbf{f}^{(i)} = \left(f_1^{(i)}, f_2^{(i)}\right)^{\mathrm{T}} \in \Re^2$ with parameter vectors $\boldsymbol{\mu}_i = \left(\mu_{i1}, \mu_{i2}, \ldots, \mu_{in}\right)^{\mathrm{T}} \in \Re^n$ is C^r-continuous ($r \geqslant 2$). In all the accessible sub-domains Ω_i, the dynamical system in Eq. (6) is continuous and the corresponding continuous flow is $\mathbf{x}^{(i)}(t) = \boldsymbol{\Phi}^{(i)}(\mathbf{x}^{(i)}(t_0), t, \boldsymbol{\mu}_i, \boldsymbol{\pi})$ with $\mathbf{x}^{(i)}(t_0) = \boldsymbol{\Phi}^{(i)}\left(\mathbf{x}^{(i)}(t_0), t_0, \boldsymbol{\mu}_i, \boldsymbol{\pi}\right)$ accordingly.

The non-smooth dynamic system theory holds for the following conditions

A1. The switching between two adjacent sub-systems possesses time continuity.

A2. In an unbounded, accessible sub-domain Ω_i, for the bounded domain $D_i \subset \Omega_i$, the corresponding vector field and its flow are bounded, i.e.,

$$\left\|\mathbf{F}_i^{(i)}\right\| \leqslant K_1 \text{ (const) and } \left\|\boldsymbol{\Phi}_i^{(i)}\right\| \leqslant K_2 \text{ (const) on } D_i \quad \text{for } t \in [0, \infty). \tag{7}$$

A3. In a bounded, accessible domain Ω_i, for the bounded domain $D_i \subseteq \Omega_i$, the corresponding vector field is bounded, but the flow may be unbounded, i.e.,

$$\left\|\mathbf{F}_i^{(i)}\right\| \leqslant K_1 \text{ (const) and } \left\|\boldsymbol{\Phi}_i^{(i)}\right\| \leqslant \infty \text{ on } D_i \quad \text{for } t \in [0, \infty). \tag{8}$$

As in Ref. [33], the real (or true) and imaginary (or fictitious) flows concepts are re-stated herein. The real (or true) flow $\mathbf{x}_i^{(i)}(t)$ in the sub-domain Ω_i is governed by the dynamical system on its own domain. The definition is given as follows.

Definition 1. The C^{r+1} continuous flow $\mathbf{x}_i^{(i)}(t) = \mathbf{\Phi}^{(i)}\left(\mathbf{x}_i^{(i)}(t_0), t, \boldsymbol{\mu}_i\right)$ is a real (or true) flow in the ith open sub-domain Ω_i, if the flow $\mathbf{x}_i^{(i)}(t)$ is determined by a C^r -continuous system ($r \geqslant 1$) on Ω_i in a form of

$$\dot{\mathbf{x}}_i^{(i)} \equiv \mathbf{F}^{(i)}\left(\mathbf{x}_i^{(i)}, t, \boldsymbol{\mu}_i\right) \in \Re^2, \quad \mathbf{x}_i^{(i)} = \left(x_i^{(i)}, y_i^{(i)}\right)^{\mathrm{T}} \in \Omega_i, \tag{9}$$

with the initial condition

$$\mathbf{x}_i^{(i)}(t_0) = \mathbf{\Phi}^{(i)}\left(\mathbf{x}_i^{(i)}(t_0), t_0, \boldsymbol{\mu}_i\right). \tag{10}$$

In the sub-domains Ω_i, $\mathbf{F}^{(i)}\left(\mathbf{x}_i^{(i)}, t, \boldsymbol{\mu}_i\right) \equiv \mathbf{F}_i^{(i)}(t)$. $\mathbf{\Phi}^{(i)}\left(\mathbf{x}_i^{(i)}(t), t_0, \boldsymbol{\mu}_i\right) \equiv \mathbf{\Phi}_i^{(i)}(t)$. $\mathbf{x}_i^{(i)}(t)$ denotes the flow in the ith sub-domain Ω_i, governed by a dynamical system defined on the ith sub-domain Ω_i. Consider the jth imaginary (or fictitious) flow in the ith domain Ω_i is a flow in Ω_i governed by the dynamical system defined on the jth-sub-domain Ω_j. The flow is not a true one governed by the non-smooth dynamical system, thus this flow is also termed the *imaginary* (or fictitious) flow in this sense.

Definition 2. The $C^{r+1}(r \geqslant 1)$-continuous flow $\mathbf{x}_i^{(j)}(t)$ is termed the jth-imaginary (or fictitious) flow in the ith open sub-domain Ω_i if the flow $\mathbf{x}_i^{(j)}(t)$ is determined by application of a C^r-continuous system, defined on the jth open sub-domain Ω_j, to the ith open sub-domain Ω_i, i.e.,

$$\dot{\mathbf{x}}_i^{(j)} \equiv \mathbf{F}^{(j)}\left(\mathbf{x}_i^{(j)}, t, \boldsymbol{\mu}_j\right) \in \Re^2, \quad \mathbf{x}_i^{(j)} = \left(x_i^{(j)}, y_i^{(j)}\right)^{\mathrm{T}} \in \Omega_i, \tag{11}$$

with the initial conditions

$$\mathbf{x}_i^{(j)}(t_0) = \mathbf{\Phi}^{(j)}\left(\mathbf{x}_i^{(j)}(t_0), t_0, \boldsymbol{\mu}_j\right). \tag{12}$$

Consider a boundary of any two adjacent sub-domains, formed by the intersection of the sub-domains, i.e., $\partial\Omega_{ij} = \overline{\Omega}_i \cap \overline{\Omega}_j$ $(i, j \in, \{1, 2, \ldots, n\}, j \neq 1)$, as shown in Fig. 3. In phase space, the separation boundary is assumed to be determined by $\varphi_{ij}(x, y) = 0$ where φ_{ij} is a C^1-continuous function.

Definition 3. The boundary set in the 2-D phase space is defined as

$$\partial\Omega_{ij} = \bar{\Omega}_i \cap \bar{\Omega}_j \equiv \left\{(x, y) \middle| \varphi_{ij}(x, y) = 0 \text{ where } \varphi_{ij} \text{ is } C^1\text{-continuous}\right\} \subset \Re^1. \tag{13}$$

Definition 4. For a discontinuous dynamical system in Eq. (9) or (11), $\mathbf{x}(t_m) \equiv \mathbf{x}_m \in \partial\Omega_{ij}$ at t_m. For an arbitrarily small $\varepsilon > 0$, there are two time intervals $[t_{m-\varepsilon}, t_m)$ and $(t_m, t_{m+\varepsilon}]$ with $\mathbf{x}_i^{(\alpha)}(t_{m-}) = \mathbf{x}_m = \mathbf{x}_j^{(\beta)}(t_{m+})$ $(\alpha, \beta \in \{i, j\}$ and $\alpha \neq \beta)$. The non-empty boundary $\partial\Omega_{ij}$ to a real or imaginary flow $\mathbf{x}_i^{(\alpha)}(t) \cup \mathbf{x}_j^{(\beta)}(t) \cup \mathbf{x}_m$ is semi-passable from the domain Ω_i to Ω_j (expressed by $\overrightarrow{\partial\Omega}_{ij}$) if the flow

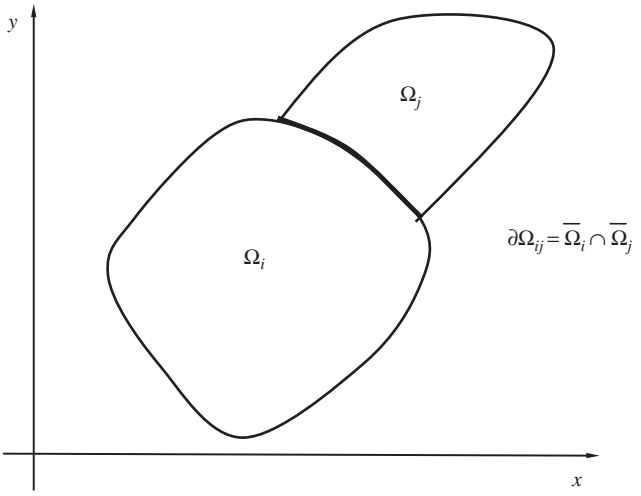

Fig. 3. Sub-domains Ω_i and Ω_j, the corresponding boundary $\partial\Omega_{ij}$ in phase space.

$\mathbf{x}_i^{(\alpha)}(t)$ and $\mathbf{x}_j^{(\beta)}(t)$ possesses the following properties:

$$\left.\begin{aligned}&\text{either}\\ &\mathbf{n}_{\partial\Omega_{ij}}^{\mathrm{T}}\bullet\left[\mathbf{x}_i^{(\alpha)}(t_{m-})-\mathbf{x}_i^{(\alpha)}(t_{m-\varepsilon})\right]>0\\ &\mathbf{n}_{\partial\Omega_{ij}}^{\mathrm{T}}\bullet\left[\mathbf{x}_j^{(\beta)}(t_{m+\varepsilon})-\mathbf{x}_j^{(\beta)}(t_{m+})\right]>0\end{aligned}\right\}\ \text{for } \partial\Omega_{ij} \text{ convex to } \Omega_j$$

$$\left.\begin{aligned}&\text{or}\\ &\mathbf{n}_{\partial\Omega_{ij}}^{\mathrm{T}}\bullet\left[\mathbf{x}_i^{(\alpha)}(t_{m-})-\mathbf{x}_i^{(\alpha)}(t_{m-\varepsilon})\right]<0\\ &\mathbf{n}_{\partial\Omega_{ij}}^{\mathrm{T}}\bullet\left[\mathbf{x}_j^{(\beta)}(t_{m+\varepsilon})-\mathbf{x}_j^{(\beta)}(t_{m+})\right]<0\end{aligned}\right\}\ \text{for } \partial\Omega_{ij} \text{ convex to } \Omega_i, \tag{14}$$

where the normal vector of the boundary $\partial\Omega_{ij}$ is

$$\mathbf{n}_{\partial\Omega_{ij}}=\nabla\varphi_{ij}=\left(\frac{\partial\varphi_{ij}}{\partial x},\frac{\partial\varphi_{ij}}{\partial y}\right)^{\mathrm{T}}_{(x_m,y_m)}. \tag{15}$$

Note that notations $t_{m\pm\varepsilon}=t_m\pm\varepsilon$ and $t_{m\pm}=t_m\pm 0$ are used. Consider a true flow in Eq. (9) from the domain Ω_i into the domain Ω_j through the boundary $\partial\Omega_{ij}$. Suppose the true flow arrives to the boundary $\partial\Omega_{ij}$ for a time t_m. For an arbitrarily small $\varepsilon>0$, a small neighborhood $(t_{m-\varepsilon},t_{m+\varepsilon})$ of the time t_m is arbitrarily selected where $t_{m\pm\varepsilon}=t_m\pm\varepsilon$. The input and output flow vectors are $\mathbf{x}_i^{(i)}(t_m)-\mathbf{x}_i^{(i)}(t_{m-\varepsilon})$ and $\mathbf{x}_j^{(j)}(t_{m+\varepsilon})-\mathbf{x}_j^{(j)}(t_m)$, respectively. As $\varepsilon\to 0$, the time increment $\Delta t\equiv\varepsilon\to 0$. The process of the flow passing through the convex and non-convex boundary sets from the domain Ω_i to Ω_j is shown in Fig. 4. Non-stick motion exists on this kind of boundary. Similarly, the geometric interpretation can be presented through the imaginary (or fictitious) flow as in Ref. [33].

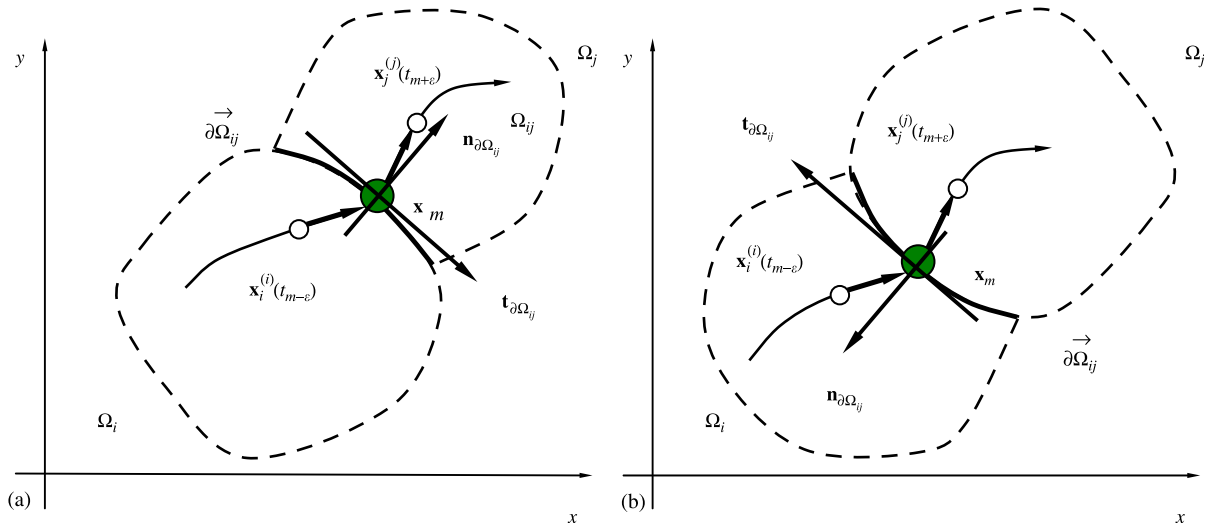

Fig. 4. Semi-passable boundary set $\overrightarrow{\partial\Omega}_{ij}$ from the domain Ω_i to Ω_j: (a) convex to Ω_j and (b) convex to Ω_i. $\mathbf{x}_i^{(i)}(t_{m-\varepsilon}) \equiv \left(x_i^{(i)}(t_{m-\varepsilon}), y_i^{(i)}(t_{m-\varepsilon})\right)^{\mathrm{T}}$, $\mathbf{x}_j^{(j)}(t_{m+\varepsilon}) \equiv \left(x_j^{(j)}(t_{m+\varepsilon}), y_j^{(j)}(t_{m+\varepsilon})\right)^{\mathrm{T}}$ and $\mathbf{x}_m \equiv (x(t_m), y(t_m))^{\mathrm{T}}$ where $t_{m\pm\varepsilon} = t_m \pm \varepsilon$ for an arbitrary small $\varepsilon > 0$. Two vectors $\mathbf{n}_{\partial\Omega_{ij}}$ and $\mathbf{t}_{\partial\Omega_{ij}}$ are the normal and tangential vectors of the boundary curve $\partial\Omega_{ij}$ determined by $\varphi_{ij}(x, y) = 0$. The direction of $\mathbf{t}_{\partial\Omega_{ij}} \times \mathbf{n}_{\partial\Omega_{ij}}$ is the positive direction of the coordinate by the right-hand rule.

Theorem 1. *For a discontinuous dynamical system in Eq.* (9) *or* (11), $\mathbf{x}(t_m) \equiv \mathbf{x}_m \in \partial\Omega_{ij}$ *for* t_m. *For an arbitrarily small* $\varepsilon > 0$, *there are two time intervals* $[t_{m-\varepsilon}, t_m)$ *and* $(t_m, t_{m+\varepsilon}]$ *with* $\mathbf{x}_i^{(\alpha)}(t_{m-}) = \mathbf{x}_m = \mathbf{x}_j^{(\beta)}(t_{m+})$ $(\alpha, \beta \in \{i, j\}$ *and* $\alpha \neq \beta)$. *Both the flows* $\mathbf{x}_i^{(\alpha)}(t)$ *and* $\mathbf{x}_j^{(\beta)}(t)$, *respectively, are* $C^r_{[t_{m-\varepsilon}, t_m)}$ *and* $C^r_{(t_m, t_{m+\varepsilon}]}$*-continuous* $(r \geqslant 2)$ *for time* t. $\left\|\mathrm{d}^r\mathbf{x}_i^{(\alpha)}/\mathrm{d}t^r\right\| < \infty$ *and* $\left\|\mathrm{d}^r\mathbf{x}_j^{(\beta)}/\mathrm{d}t^r\right\| < \infty$. *So that the non-empty boundary set* $\partial\Omega_{ij}$ *is semi-passable from the domain* Ω_i *to* Ω_j *iff*

either

$$\mathbf{n}^{\mathrm{T}}_{\partial\Omega_{ij}} \bullet \dot{\mathbf{x}}_i^{(\alpha)}(t_{m-}) > 0 \text{ and } \mathbf{n}^{\mathrm{T}}_{\partial\Omega_{ij}} \bullet \dot{\mathbf{x}}_j^{(\beta)}(t_{m+}) > 0 \text{ for } \partial\Omega_{ij} \text{ convex to } \Omega_j$$

or

$$\mathbf{n}^{\mathrm{T}}_{\partial\Omega_{ij}} \bullet \dot{\mathbf{x}}_i^{(\alpha)}(t_{m-}) < 0 \text{ and } \mathbf{n}^{\mathrm{T}}_{\partial\Omega_{ij}} \bullet \dot{\mathbf{x}}_j^{(\beta)}(t_{m+}) < 0 \text{ for } \partial\Omega_{ij} \text{ convex to } \Omega_i. \tag{16}$$

Theorem 2. *For a discontinuous dynamical system in Eq.* (9) *or* (11), $\mathbf{x}(t_m) \equiv \mathbf{x}_m \in \partial\Omega_{ij}$ *for* t_m. *For an arbitrarily small* $\varepsilon > 0$, *there are two time intervals* $[t_{m-\varepsilon}, t_m)$ *and* $(t_m, t_{m+\varepsilon}]$ *with* $\mathbf{x}_i^{(\alpha)}(t_{m-}) = \mathbf{x}_m = \mathbf{x}_j^{(\beta)}(t_{m+})$ $(\alpha, \beta \in \{i, j\}$ *and* $\alpha \neq \beta)$. *Both* $\mathbf{F}_i^{(\alpha)}(t)$ *and* $\mathbf{F}_j^{(\beta)}(t)$, *respectively, are* $C^r_{[t_{m-\varepsilon}, t_m)}$ *and* $C^r_{(t_m, t_{m+\varepsilon}]}$*-continuous* $(r \geqslant 1)$ *for time* t. $\left\|\mathrm{d}^r\mathbf{x}_\alpha^{(\alpha)}/\mathrm{d}t^r\right\| < \infty$ *and* $\left\|\mathrm{d}^r\mathbf{x}_\alpha^{(\beta)}/\mathrm{d}t^r\right\| < \infty$. *So that the non-empty boundary set* $\partial\Omega_{ij}$ *is semi-passable from the domain* Ω_i *to* Ω_j *iff*

either

$$\mathbf{n}^{\mathrm{T}}_{\partial\Omega_{ij}} \bullet \mathbf{F}_i^{(\alpha)}(t_{m-}) > 0 \text{ and } \mathbf{n}^{\mathrm{T}}_{\partial\Omega_{ij}} \bullet \mathbf{F}_j^{(\beta)}(t_{m+}) > 0 \text{ for } \partial\Omega_{ij} \text{ convex to } \Omega_j,$$

or

$$\mathbf{n}^{\mathrm{T}}_{\partial\Omega_{ij}} \bullet \mathbf{F}^{(\alpha)}_i(t_{m-}) < 0 \text{ and } \mathbf{n}^{\mathrm{T}}_{\partial\Omega_{ij}} \bullet \mathbf{F}^{(\beta)}_j(t_{m+}) < 0 \text{ for } \partial\Omega_{ij} \text{ convex to } \Omega_i \tag{17}$$

where $\mathbf{F}^{(\alpha)}_i(t_{m-}) = \mathbf{F}^{(\alpha)}\left(\mathbf{x}^{(\alpha)}_i, t_{m-}, \boldsymbol{\mu}_i\right)$ *and* $\mathbf{F}^{(\beta)}_j(t_{m+}) = \mathbf{F}^{(\beta)}\left(\mathbf{x}^{(\beta)}_j, t_{m+}, \boldsymbol{\mu}_\beta\right)$.

Definition 5. For a discontinuous dynamical system in Eq. (9) or (11), $\mathbf{x}(t_m) \equiv \mathbf{x}_m \in \partial\Omega_{ij}$ for t_m. For an arbitrarily small $\varepsilon > 0$, there is a time interval $[t_{m-\varepsilon}, t_m)$ with $\mathbf{x}^{(\alpha)}_\alpha(t_{m-}) = \mathbf{x}_m = \mathbf{x}^{(\beta)}_\alpha(t_{m+})$ $(\alpha, \beta \in \{i, j\}, \alpha \neq \beta)$. The non-empty boundary set $\partial\Omega_{ij}$ is the non-passable boundary of the first kind, $\widetilde{\partial\Omega_{ij}}$ (or termed a sink boundary between the sub-domains Ω_i and Ω_j) if the flows $\mathbf{x}^{(\beta)}_\alpha(t)$ in the neighborhood of the boundary $\partial\Omega_{ij}$ possess the following property:

$$\left\{\mathbf{n}^{\mathrm{T}}_{\partial\Omega_{ij}} \bullet \left[\mathbf{x}^{(i)}_i(t_{m-}) - \mathbf{x}^{(i)}_i(t_{m-\varepsilon})\right]\right\} \times \left\{\mathbf{n}^{\mathrm{T}}_{\partial\Omega_{ij}} \bullet \left[\mathbf{x}^{(j)}_j(t_{m-}) - \mathbf{x}^{(j)}_j(t_{m-\varepsilon})\right]\right\} < 0$$

or

$$\left\{\mathbf{n}^{\mathrm{T}}_{\partial\Omega_{ij}} \bullet \left[\mathbf{x}^{(j)}_i(t_{m+\varepsilon}) - \mathbf{x}^{(j)}_i(t_{m+})\right]\right\} \times \left\{\mathbf{n}^{\mathrm{T}}_{\partial\Omega_{ij}} \bullet \left[\mathbf{x}^{(i)}_j(t_{m+\varepsilon}) - \mathbf{x}^{(i)}_j(t_{m+})\right]\right\} < 0. \tag{18}$$

The sink boundary between the two sub-domains Ω_i and Ω_j is sketched in Fig. 5 through the real (or true) flow $\mathbf{x}^{(\alpha)}_\alpha(t)$, $\alpha \in \{i, j\}$. In the neighborhood of the boundary, when a flow $\mathbf{x}^{(\alpha)}_\alpha(t)$ in the domain Ω_α arrives to the non-passable boundary of the first kind $\widetilde{\partial\Omega_{ij}}$, the flow can be tangential to or sliding on the non-passable boundary. For the sink boundary, the stick motion will exist. However, the tangential case will be discussed later. As in Ref. [32], the following theorems are given for determination of the sink separation boundary. Namely, the existence of the stick motion will be guaranteed.

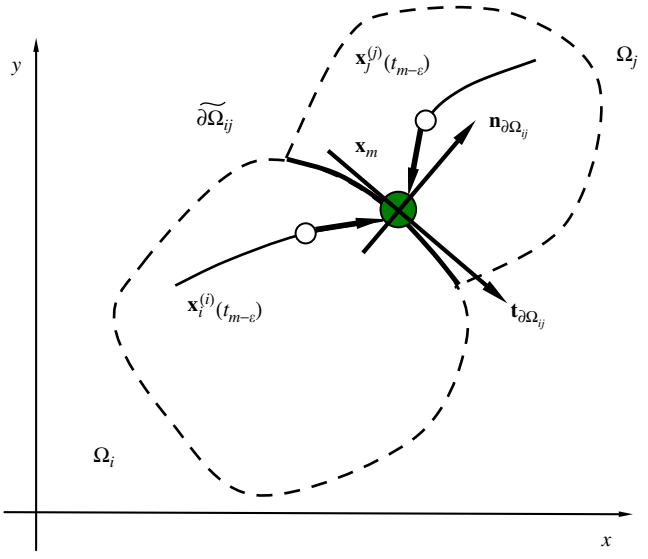

Fig. 5. The sink boundary (or the non-passable boundary of the first kind, $\widetilde{\partial\Omega_{ij}}$). $\mathbf{x}_m \equiv (x(t_m), y(t_m))^{\mathrm{T}}$, $\mathbf{x}^{(\alpha)}_\alpha(t_{m-\varepsilon}) \equiv \left(x^{(\alpha)}_\alpha(t_{m-\varepsilon}), y^{(\alpha)}_\alpha(t_{m-\varepsilon})\right)^{\mathrm{T}}$ where $t_{m-\varepsilon} = t_m - \varepsilon$ for an arbitrary small $\varepsilon > 0$. Two vectors $\mathbf{n}_{\partial\Omega_{ij}}$ and $\mathbf{t}_{\partial\Omega_{ij}}$ are the normal and tangential vectors of the boundary curve $\partial\Omega_{ij}$ determined by $\varphi_{ij}(x, y) = 0$. The direction of $\mathbf{t}_{\partial\Omega_{ij}} \times \mathbf{n}_{\partial\Omega_{ij}}$ is the positive direction of the coordinate by the right-hand rule.

Theorem 3. *For a discontinuous dynamical system in Eq.* (9) *or* (11), $\mathbf{x}(t_m) \equiv \mathbf{x}_m \in \partial\Omega_{ij}$ *for* t_m. *For an arbitrarily small* $\varepsilon > 0$, *there is a time interval* $[t_{m-\varepsilon}, t_m)$ *or* $(t_m, t_{m+\varepsilon}]$ *with* $\mathbf{x}_\alpha^{(\alpha)}(t_{m-}) = \mathbf{x}_m = \mathbf{x}_\alpha^{(\beta)}(t_{m+})$ $(\alpha, \beta \in \{i,j\}, \alpha \neq \beta)$. *The flows* $\mathbf{x}_\alpha^{(\alpha)}(t)$ *and* $\mathbf{x}_\alpha^{(\beta)}(t)$ *in the two domains are* $C^r_{[t_{m-\varepsilon},t_m)}$ *and* $C^r_{(t_m,t_{m+\varepsilon}]}$*-continuous* $(r \geqslant 2)$ *for time t, respectively,* $\left\|\mathrm{d}^r\mathbf{x}_\alpha^{(\alpha)}/\mathrm{d}t^r\right\| < \infty$, *and* $\left\|\mathrm{d}^r\mathbf{x}_\alpha^{(\beta)}/\mathrm{d}t^r\right\| < \infty$. *So that the non-empty boundary* $\partial\Omega_{ij}$ *is a non-passable boundary of the first kind iff*

$$\left[\mathbf{n}^{\mathrm{T}}_{\partial\Omega_{ij}} \bullet \dot{\mathbf{x}}_i^{(i)}(t_{m-})\right] \times \left[\mathbf{n}^{\mathrm{T}}_{\partial\Omega_{ij}} \bullet \dot{\mathbf{x}}_j^{(j)}(t_{m-})\right] < 0$$

or

$$\left[\mathbf{n}^{\mathrm{T}}_{\partial\Omega_{ij}} \bullet \dot{\mathbf{x}}_i^{(j)}(t_{m+})\right] \times \left[\mathbf{n}^{\mathrm{T}}_{\partial\Omega_{ij}} \bullet \mathbf{x}_j^{(i)}(t_{m+})\right] < 0. \tag{19}$$

Theorem 4. *For a discontinuous dynamical system in Eq.* (6), $\mathbf{x}(t_m) \equiv \mathbf{x}_m \in \partial\Omega_{ij}$ *for* t_m. *For an arbitrarily small* $\varepsilon > 0$, *there is a time interval* $[t_{m-\varepsilon}, t_m)$ *with* $\mathbf{x}_\alpha^{(\alpha)}(t_{m-}) = \mathbf{x}_m = \mathbf{x}_\alpha^{(\beta)}(t_{m+})$ $(\alpha, \beta \in \{i,j\}, \alpha \neq \beta)$. *The vector field* $\mathbf{F}_\alpha^{(\alpha)}(t)$ *and* $\mathbf{F}_\alpha^{(\beta)}(t)$ *in the two domains are* $C^r_{[t_{m-\varepsilon},t_m)}$ *and* $C^r_{(t_m,t_{m+\varepsilon}]}$*-continuous* $(r \geqslant 2)$ *for time t, respectively,* $\left\|\mathrm{d}^{r+1}\mathbf{x}_\alpha^{(\alpha)}/\mathrm{d}t^{r+1}\right\| < \infty$ *and* $\left\|\mathrm{d}^{r+1}\mathbf{x}_\alpha^{(\beta)}/\mathrm{d}t^{r+1}\right\| < \infty$. *So that the non-empty boundary* $\partial\Omega_{ij}$ *is a non-passable boundary of the first kind iff*

$$\left[\mathbf{n}^{\mathrm{T}}_{\partial\Omega_{ij}} \bullet \mathbf{F}_i^{(i)}(t_{m-})\right] \times \left[\mathbf{n}^{\mathrm{T}}_{\partial\Omega_{ij}} \bullet \mathbf{F}_j^{(j)}(t_{m-})\right] < 0$$

or

$$\left[\mathbf{n}^{\mathrm{T}}_{\partial\Omega_{ij}} \bullet \mathbf{F}_i^{(j)}(t_{m+})\right] \times \left[\mathbf{n}^{\mathrm{T}}_{\partial\Omega_{ij}} \bullet \mathbf{F}_j^{(i)}(t_{m+})\right] < 0 \tag{20}$$

where $\mathbf{F}_\alpha^{(\alpha)}(t_{m-}) \triangleq \mathbf{F}^{(\alpha)}\left(\mathbf{x}_\alpha^{(\alpha)}, t_{m-}, \boldsymbol{\mu}_\alpha\right)$ *and* $\mathbf{F}_\alpha^{(\beta)}(t_{m+}) \triangleq \mathbf{F}^{(\beta)}\left(\mathbf{x}_\alpha^{(\beta)}, t_{m+}, \boldsymbol{\mu}_\beta\right)$.

As in Ref. [32], the flows tangential to the separation boundary are presented herein in order to investigate the grazing bifurcation at the boundary.

Definition 6. For a discontinuous dynamical system in Eq. (9) or (11), $\mathbf{x}(t_m) \equiv \mathbf{x}_m \in \partial\Omega_{ij}$ at t_m. For an arbitrarily small $\varepsilon > 0$, there is a time interval $[t_{m-\varepsilon}, t_m)$ with $\mathbf{x}_\alpha^{(\beta)}(t_{m\pm}) = \mathbf{x}_m$ $(\alpha, \beta \in \{i,j\}, \alpha \neq \beta)$. The flow $\mathbf{x}_\alpha^{(\beta)}(t)$ in Ω_α at (x_m, y_m) is tangential to the boundary $\partial\Omega_{ij}$ if the following two conditions hold:

$$\text{(C1)} \qquad \mathbf{n}^{\mathrm{T}}_{\partial\Omega_{ij}} \bullet \dot{\mathbf{x}}_\alpha^{(\beta)}(t_{m\pm}) = 0, \tag{21}$$

$$\text{(C2)} \qquad \left\{\mathbf{n}^{\mathrm{T}}_{\partial\Omega_{ij}} \bullet \left[\mathbf{x}_\alpha^{(\beta)}(t_m) - \mathbf{x}_\alpha^{(\beta)}(t_{m-\varepsilon})\right]\right\} \times \left\{\mathbf{n}^{\mathrm{T}}_{\partial\Omega_{ij}} \bullet \left[\mathbf{x}_\alpha^{(\beta)}(t_{m+\varepsilon}) - \mathbf{x}_\alpha^{(\beta)}(t_m)\right]\right\} < 0. \tag{22}$$

This tangential bifurcation is often termed the grazing bifurcation. As in Ref. [32], the following theorems are presented for determination of the tangential bifurcation at the separation boundary. The graphical illustration of such a definition is given in Fig. 6.

Theorem 5. *For a discontinuous dynamical system in Eq.* (6), $\mathbf{x}(t_m) \equiv \mathbf{x}_m \in \partial\Omega_{ij}$ *for* t_m. *For an arbitrarily small* $\varepsilon > 0$, *there is a time interval* $[t_{m-\varepsilon}, t_{m+\varepsilon}]$ *with* $\mathbf{x}_\alpha^{(\beta)}(t_{m\pm}) = \mathbf{x}_m$ $(\alpha, \beta \in \{i,j\})$. *The two segment flows* $\mathbf{x}_\alpha^{(\beta)}(t)$ *are* $C^r_{[t_{m-\varepsilon},t_m)}$ *and* $C^r_{(t_m,t_{m+\varepsilon}]}$*-continuous* $(r \geqslant 2)$ *for time t.* $\left\|\mathrm{d}^r\mathbf{x}_\alpha^{(\beta)}/\mathrm{d}t^r\right\| < \infty$.

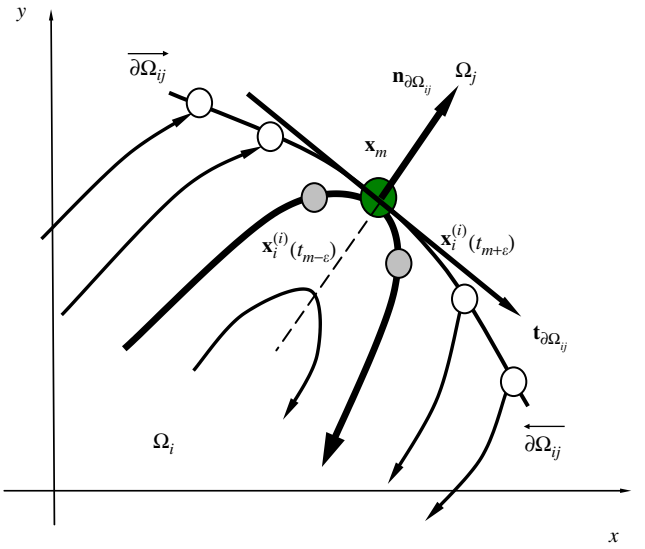

Fig. 6. A flow in the domain Ω_i tangential to the boundary $\partial\Omega_{ij}$ convex to Ω_j. The gray-filled symbols represent two points $\left(\mathbf{x}_\alpha^{(\alpha)}(t_{m\pm\varepsilon})\right)$ on the flow before and after the tangency. The tangential point $\mathbf{x}_m$ on the boundary $\partial\Omega_{ij}$ is depicted by a large circular symbol. $\mathbf{n}_{\partial\Omega_{ij}}$ and $\mathbf{t}_{\partial\Omega_{ij}}$ are the normal and tangential direction of the boundary $\partial\Omega_{ij}$. The direction of $\mathbf{t}_{\partial\Omega_{ij}} \times \mathbf{n}_{\partial\Omega_{ij}}$ is the positive direction of the coordinate by the right-hand rule.

So that the flow $\mathbf{x}_\alpha^{(\beta)}(t)$ *in* $\partial\Omega_\alpha$ *at* (x_m, y_m) *is tangential to the boundary* $\partial\Omega_{ij}$ *if the two conditions hold*:

$$\text{(C1)} \qquad \mathbf{n}_{\partial\Omega_{ij}}^{\mathrm{T}} \bullet \dot{\mathbf{x}}_\alpha^{(\beta)}(t_{m\pm}) = 0 \text{ or } \mathbf{n}_{\partial\Omega_{ij}}^{\mathrm{T}} \bullet \mathbf{F}_\alpha^{(\beta)}\left(\mathbf{x}_\alpha^{(\beta)}, t_{m\pm}, \boldsymbol{\mu}_\beta, \boldsymbol{\pi}\right) = 0;$$

$$\text{(C2) } \textit{either} \tag{23}$$

$$\left[\mathbf{n}_{\partial\Omega_{ij}}^{\mathrm{T}} \bullet \dot{\mathbf{x}}_\alpha^{(\beta)}(t_{m-\varepsilon})\right] \times \left[\mathbf{n}_{\partial\Omega_{ij}}^{\mathrm{T}} \bullet \dot{\mathbf{x}}_\alpha^{(\beta)}(t_{m+\varepsilon})\right] < 0 \tag{24}$$

or

$$\left[\mathbf{n}_{\partial\Omega_{ij}}^{\mathrm{T}} \bullet \mathbf{F}_\alpha^{(\beta)}\left(\mathbf{x}_\alpha^{(\beta)}, t_{m-\varepsilon}, \boldsymbol{\mu}_\beta, \boldsymbol{\pi}\right)\right] \times \left[\mathbf{n}_{\partial\Omega_{ij}}^{\mathrm{T}} \bullet \mathbf{F}_\alpha^{(\beta)}\left(\mathbf{x}_\alpha^{(\beta)}, t_{m+\varepsilon}, \boldsymbol{\mu}_\beta, \boldsymbol{\pi}\right)\right] < 0. \tag{25}$$

For convenience, the following theorem can be used for determination of the tangential (or grazing) bifurcation on the separation boundary. The theorem is stated as follows.

Theorem 6. *For a discontinuous dynamical system in Eq.* (9) *or* (11), $\mathbf{x}(t_m) \equiv \mathbf{x}_m \in \partial\Omega_{ijj}$ *for* t_m. *For an arbitrarily small* $\varepsilon > 0$, *there is a time interval* $[t_{m-\varepsilon}, t_{m+\varepsilon}]$ *with* $\mathbf{x}_\alpha^{(\beta)}(t_{m+}) = \mathbf{x}_m$ $(\alpha, \beta \in \{i, j\})$. *The vector field* $\mathbf{F}_\alpha^{(\beta)}(t)$ *are* $C^r_{[t_{m-\varepsilon}, t_m)}$ *and* $C^r_{(t_m, t_{m+\varepsilon}]}$*-continuous* $(r \geqslant 2)$ *for time* t. $\left\|\mathrm{d}^{r+1}\mathbf{x}^{(\alpha)}/\mathrm{d}t^{r+1}\right\| < \infty$. *So that the flow* $\mathbf{x}_\alpha^{(\beta)}(t)$ *in* Ω_α *at* (x_m, y_m) *is tangential to the boundary* $\partial\Omega_{ij}$ *if the two conditions hold*:

$$\text{(C1)} \qquad \mathbf{n}_{\partial\Omega_{ij}}^{\mathrm{T}} \bullet \dot{\mathbf{x}}_\alpha^{(\beta)}(t_{m\pm}) = 0 \text{ or } \mathbf{n}_{\partial\Omega_{ij}}^{\mathrm{T}} \bullet \mathbf{F}_\alpha^{(\beta)}\left(\mathbf{x}_\alpha^{(\beta)}, t_{m\pm}, \boldsymbol{\mu}_\beta, \boldsymbol{\pi}\right) = 0; \tag{26}$$

$$\text{(C2)}\quad \left.\begin{array}{l} \textit{either } \mathbf{n}^{\mathrm{T}}_{\partial\Omega_{ij}} \bullet D\mathbf{F}^{(\beta)}_{\alpha}(t_{m\pm}) < 0 \textit{ for } \partial\Omega_{ij} \textit{ convex to } \Omega_{\beta}\ \left(\beta \in \{i,j\} \textit{ but } \beta \neq \alpha\right) \\ \textit{or } \mathbf{n}^{T}_{\partial\Omega_{ij}} \bullet D\mathbf{F}^{(\beta)}_{\alpha}(t_{m\pm}) > 0 \textit{ for } \partial\Omega_{ij} \textit{ convex to } \Omega_{\alpha}, \end{array}\right\}, \tag{27}$$

where the total differentiation

$$D\mathbf{F}^{(\beta)}_{\alpha}(t_{m\pm}) = \left[\frac{\partial F^{(\beta)}_{\alpha,p}(t_{m\pm})}{\partial x_q}\right]\mathbf{F}^{(\beta)}_{\alpha}(t_{m\pm}) + \frac{\partial \mathbf{F}^{(\beta)}_{\alpha}(t_{m\pm})}{\partial t} \quad \left(\{p,q\} = \{1,2\}, x_1 = x, x_2 = y\right). \tag{28}$$

The proof of the above theorems can be referred to Luo [32,33]. From the above theorems, the conditions for the onset, existence and disappearance of stick, non-stick and grazing motions in the friction-induced oscillators, as in Eq. (5), will be developed in the next section.

3. Force criteria

In this section, the criteria for stick and grazing motion can be applied to generalized, nonlinear oscillator with a nonlinear dry friction. As in Ref. [1], since the friction force is dependent on the direction of the relative velocity, the phase plane of the friction-induced oscillation systems is partitioned into two domains. In each domain, the motion can be described through the continuous dynamical systems, as shown in Fig. 7. The two domains are expressed by $\Omega_{\alpha}(\alpha \in \{1,2\})$. In the phase plane, the following vectors are introduced as

$$\mathbf{x} \triangleq (x,\dot{x})^{\mathrm{T}} \equiv (x,y)^{\mathrm{T}} \text{ and } \mathbf{F} \triangleq (y,F)^{\mathrm{T}}. \tag{29}$$

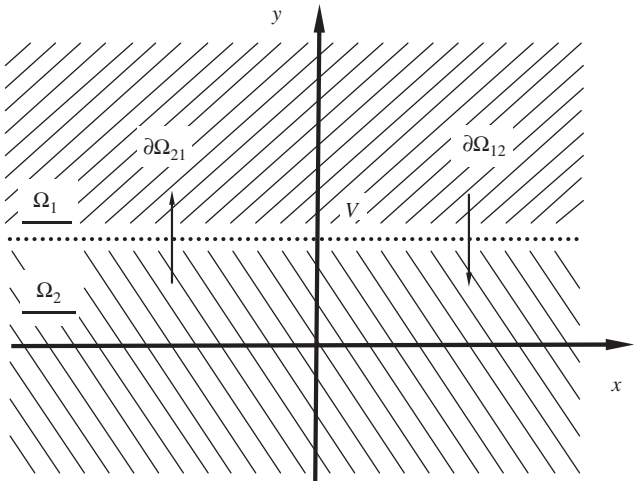

Fig. 7. Domain partitions in phase plane for constant belt speed V.

The mathematical description of the domains and boundary

$$\Omega_1 = \{(x,y)|y \in (V,\infty)\}, \quad \Omega_2 = \{(x,y)|y \in (-\infty, V)\},$$
$$\partial\Omega_{\alpha\beta} = \left\{(x,y)|\varphi_{\alpha\beta}(x,y) \equiv y - V = 0\right\}. \tag{30}$$

The subscript $(\cdot)_{\alpha\beta}$ denotes the boundary from Ω_α to Ω_β ($\alpha,\beta \in \{1,2\}$ and $\alpha \neq \beta$). The motion of equations for friction-induced oscillators, such as in Eqs. (3) and (5), can be described as

$$\dot{\mathbf{x}} = \mathbf{F}_\lambda^{(\kappa)}(\mathbf{x},t) \quad (\kappa,\lambda \in \{0,1,2\}), \tag{31}$$

where

$$\begin{aligned}
&\mathbf{F}_\alpha^{(\alpha)}(\mathbf{x},t) = (y, F_\alpha(\mathbf{x},t))^{\mathrm{T}} \text{ in } \Omega_\alpha \ (\alpha \in \{1,2\}),\\
&\mathbf{F}_\alpha^{(\alpha)}(\mathbf{x},t) = (y, F_\beta(\mathbf{x},t))^{\mathrm{T}} \text{ in } \Omega_\alpha \ (\alpha \neq \beta \in \{1,2\}),\\
&\mathbf{F}_0^{(0)}(\mathbf{x},t) = (V,0)^{\mathrm{T}} \text{ on } \partial\Omega_{\alpha\beta} \text{ for stick},\\
&\mathbf{F}_0^{(0)}(\mathbf{x},t) = \left[\mathbf{F}_\alpha^{(\alpha)}(\mathbf{x},t), \mathbf{F}_\beta^{(\beta)}(\mathbf{x},t)\right] \text{ on } \partial\Omega_{\alpha\beta} \text{ for non-stick}.
\end{aligned} \tag{32}$$

For the subscript and superscript (κ and λ) with non-zero values, they represent the two adjacent domains for $(\alpha,\beta \in \{1,2\}$. $\mathbf{F}_\alpha^{(\alpha)}(x,t)$ is the true (or real) vector field in the α-domain. $\mathbf{F}_\alpha^{(\beta)}(x,t)$ is the fictitious (or imaginary) vector field in the α-domain, which is determined by the vector field in the β-domain. $\mathbf{F}_0^{(0)}(x,t)$ is the vector field on the separation boundary, and the discontinuity of the vector field for the entire system is presented through such an expression. $F_\alpha(x,t)$ is the scalar force in the α-domain. For the system in Eq. (5), we have the forces in the two domains as

$$F_\alpha(\mathbf{x},t) = A_0 \cos \Omega t - b_\alpha - 2d_\alpha y - c_\alpha x \quad (\alpha \in \{1,2\}). \tag{33}$$

Note that $b_1 = -b_2 = \mu g$, $d_\alpha = d$ and $c_\alpha = c$ for the model in Fig. 1. From Theorem 4, the stick motion (or mathematically called the sliding motion) through the real (or true) flow is guaranteed, if $\partial\Omega_{\alpha\beta}$ ($\alpha \neq \beta$) is convex to Ω_α, by

$$\left[\mathbf{n}_{\partial\Omega_{\alpha\beta}}^{\mathrm{T}} \bullet \mathbf{F}_\alpha^{(\alpha)}(t_{m-})\right] < 0 \quad \text{and} \quad \left[\mathbf{n}_{\partial\Omega_{\alpha\beta}}^{\mathrm{T}} \bullet \mathbf{F}_\beta^{(\beta)}(t_{m-})\right] > 0. \tag{34}$$

Note that t_m represents the time for the motion on the velocity boundary, and $t_{m\pm} = t_m \pm 0$ indicates responses in the two domains rather than on the boundary. Similarly, from Theorem 2, the non-stick motion (or called passable motion to boundary in Refs. [32,33]) through the real or imaginary flows is guaranteed, if $\partial\Omega_{\alpha\beta}$ is convex to Ω_α, by

$$\begin{aligned}
&\left[\mathbf{n}_{\partial\Omega_{\alpha\beta}}^{\mathrm{T}} \bullet \mathbf{F}_\alpha^{(\alpha)}(t_{m-})\right] < 0 \text{ and } \left[\mathbf{n}_{\partial\Omega_{\alpha\beta}}^{\mathrm{T}} \bullet \mathbf{F}_\beta^{(\beta)}(t_{m+})\right] < 0 \text{ for } \Omega_\alpha \to \Omega_\beta,\\
&\left[\mathbf{n}_{\partial\Omega_{\beta\alpha}}^{\mathrm{T}} \bullet \mathbf{F}_\beta^{(\beta)}(t_{m-})\right] > 0 \text{ and } \left[\mathbf{n}_{\partial\Omega_{\beta\alpha}}^{\mathrm{T}} \bullet \mathbf{F}_\alpha^{(\alpha)}(t_{m+})\right] > 0 \text{ for } \Omega_\beta \to \Omega_\alpha.
\end{aligned}$$

or

$$\begin{aligned}
&\left[\mathbf{n}_{\partial\Omega_{\alpha\beta}}^{\mathrm{T}} \bullet \mathbf{F}_\alpha^{(\alpha)}(t_{m-})\right] < 0 \text{ and } \left[\mathbf{n}_{\partial\Omega_{\alpha\beta}}^{\mathrm{T}} \bullet \mathbf{F}_\alpha^{(\beta)}(t_{m-})\right] < 0 \text{ for } \Omega_\alpha \to \Omega_\beta,\\
&\left[\mathbf{n}_{\partial\Omega_{\beta\alpha}}^{\mathrm{T}} \bullet \mathbf{F}_\beta^{(\beta)}(t_{m-})\right] > 0 \text{ and } \left[\mathbf{n}_{\partial\Omega_{\beta\alpha}}^{\mathrm{T}} \bullet \mathbf{F}_\beta^{(\alpha)}(t_{m-})\right] > 0 \text{ for } \Omega_\beta \to \Omega_\alpha.
\end{aligned} \tag{35}$$

because of the sliding dynamics on the separation boundary, the separation boundary $\partial\Omega_{12}$ (or $\partial\Omega_{21}$) is convex to Ω_1. Using the third equation of Eq. (30), Eq. (15) gives the normal vector of the separation boundary, i.e.,

$$\mathbf{n}_{\partial\Omega_{12}} = \mathbf{n}_{\partial\Omega_{21}} = (0,1)^{\mathrm{T}}. \tag{36}$$

Therefore, we have

$$\begin{aligned} &\mathbf{n}^{\mathrm{T}}_{\partial\Omega_{\alpha\beta}} \bullet \mathbf{F}^{(\alpha)}_{\alpha}(t) = \mathbf{n}^{\mathrm{T}}_{\partial\Omega_{\beta\alpha}} \bullet \mathbf{F}^{(\alpha)}_{\alpha}(t) = F_{\alpha}(\mathbf{x},t),\\ &\mathbf{n}^{T}_{\partial\Omega_{\alpha\beta}} \bullet \mathbf{F}^{(\beta)}_{\alpha}(t) = \mathbf{n}^{\mathrm{T}}_{\partial\Omega_{\beta\alpha}} \bullet \mathbf{F}^{(\beta)}_{\alpha}(t) = F_{\beta}(\mathbf{x},t). \end{aligned} \tag{37}$$

From Eqs. (34) and (35), the force conditions for stick and non-stick motions, respectively, are:

$$\left.\begin{aligned} &F_1(t_{m-})<0 \text{ and } F_2(t_{m-})>0 \quad \text{on } \partial\Omega_{12},\\ &F_1(t_{m-})<0 \text{ and } F_2(t_{m+})<0 \quad \text{for } \Omega_1 \to \Omega_2,\\ &F_1(t_{m-})>0 \text{ and } F_2(t_{m-})>0 \quad \text{for } \Omega_2 \to \Omega_1. \end{aligned}\right\} \tag{38}$$

From the theory for non-smooth dynamical systems in Refs. [32,33], the force conditions for vanishing of the stick motions are

$$\begin{aligned} &F_1(t_{m-})<0 \text{ and } F_2(t_{m-}) = 0 \quad \text{for } \widetilde{\partial\Omega}_{12} \to \Omega_2,\\ &F_2(t_{m-})>0 \text{ and } F_1(t_{m-}) = 0 \quad \text{for } \widetilde{\partial\Omega}_{12} \to \Omega_1. \end{aligned} \tag{39}$$

From Eq. (35), the onset condition for the sliding motion is

$$\begin{aligned} &F_1(t_{m-})<0 \text{ and } F_2(t_{m+}) = 0 \quad \text{for } \Omega_1 \to \widetilde{\partial\Omega}_{12},\\ &F_2(t_{m-})>0 \text{ and } F_1(t_{m+}) = 0 \quad \text{for } \Omega_2 \to \widetilde{\partial\Omega}_{12}. \end{aligned} \tag{40}$$

The onset condition of the sliding motion is also called the *sliding* bifurcation condition, and the detailed discussion can be referred to Luo and Gegg [34]. A sketch of the stick motion is presented in Fig. 8. In Fig. 8(a), the force condition for the sliding motion with its vanishing and appearance is presented through the vector fields of $\mathbf{F}^{(1)}_1(t)$ and $\mathbf{F}^{(2)}_2(t)$. The vanishing condition for stick (or sliding) motion along the velocity boundary is illustrated by $F_2(t_{m-}) = 0$. The vanishing point is labeled by the gray circular symbol. However, the starting points of the sliding motion may not be the switching points from the possible boundary to the non-passable motion boundary. The switching point satisfies the onset condition of the sliding motion in Eq. (40). When the flow arrives to the separation boundary, once the first equation of Eq. (38) holds, the sliding motion along the corresponding discontinuous boundary will be formed. The onset of the sliding motion from the domain Ω_2 onto the sliding boundary $\widetilde{\partial\Omega}_{12}$ is labeled by the dark circular symbol in Fig. 8(b). From Eq. (40), $F_1(t_{m+}) = 0$ should be hold.

From Theorem 6, the grazing motion is guaranteed by

$$\begin{aligned} &\left[\mathbf{n}^{\mathrm{T}}_{\partial\Omega_{\alpha\beta}} \bullet \mathbf{F}^{(\alpha)}_{\alpha}(t_{m\pm})\right] = 0,\\ &\left[\mathbf{n}^{\mathrm{T}}_{\partial\Omega_{12}} \bullet DF^{(1)}_1(t_{m\pm})\right] > 0, \quad \left[\mathbf{n}^{\mathrm{T}}_{\partial\Omega_{21}} \bullet D\mathbf{F}^{(2)}_2(t_{m\pm})\right] < 0, \end{aligned} \tag{41}$$

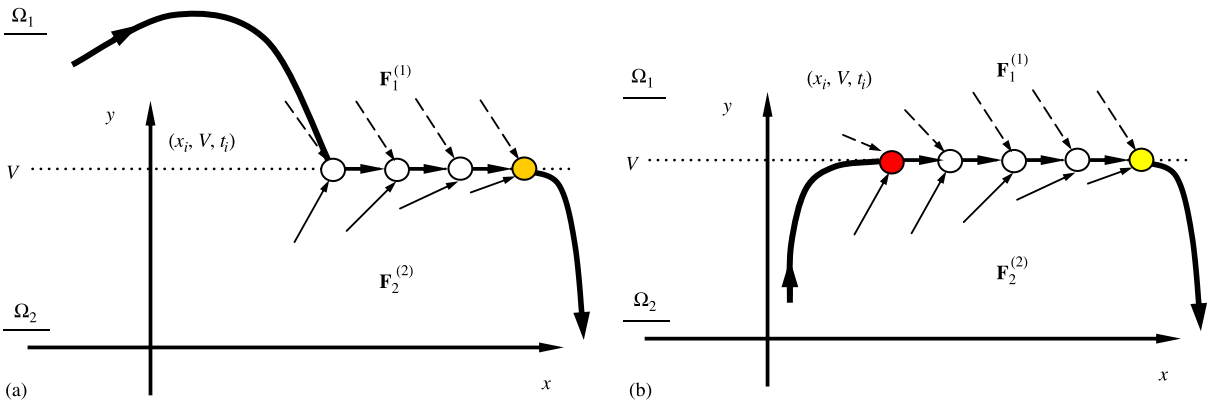

Fig. 8. Vector fields of stick motion with (a) vanishing only, and (b) onset and vanishing for belt speed $V>0$. The gray and dark filled circular symbols represent the vanishing and onset of stick motion, respectively.

where

$$D\mathbf{F}_{\alpha}^{(\alpha)}(t)=\left(2F_{\alpha}(\mathbf{x},t),\nabla F_{\alpha}(\mathbf{x},t)\bullet\mathbf{F}_{\alpha}^{(\alpha)}(t)+\frac{\partial F_{\alpha}(\mathbf{x},t)}{\partial t}\right)^{\mathrm{T}}, \tag{42}$$

where $\nabla=\partial/\partial x\mathbf{i}+\partial/\partial y\mathbf{j}$ is the Hamilton operator. With Eqs. (32) and (36), we have

$$\begin{aligned}&\mathbf{n}_{\partial\Omega_{\alpha\beta}}^{\mathrm{T}}\bullet\mathbf{F}_{\alpha}^{(\alpha)}(t)=F_{\alpha}(\mathbf{x},\Omega t),\\&\mathbf{n}_{\partial\Omega_{\alpha\beta}}^{T}\bullet D\mathbf{F}_{\alpha}^{(\alpha)}(t)=\nabla F_{\alpha}(\mathbf{x},\Omega t)\bullet\mathbf{F}_{\alpha}^{(\alpha)}(t)+\frac{\partial F_{\alpha}(\mathbf{x},\Omega t)}{\partial t}.\end{aligned} \tag{43}$$

From Eqs. (42) and (43), the force conditions for grazing motions are:

$$F_{\alpha}(\mathbf{x}_m,\Omega t_{m\pm})=0,\quad F_{\alpha}(\mathbf{x}_m,\Omega t_{m-\varepsilon})\times F_{\alpha}(\mathbf{x}_m,\Omega t_{m+\varepsilon})<0 \tag{44}$$

or

$$F_{\alpha}(\mathbf{x}_m,\Omega t_{m\pm})=0,\quad \nabla F_{\alpha}(\mathbf{x}_m,\Omega t_{m\pm})\bullet\mathbf{F}_{\alpha}^{(\alpha)}(t_{m\pm})+\frac{\partial F_{\alpha}(\mathbf{x}_m,\Omega t_{m\pm})}{\partial t}\begin{cases}>0 & \text{for } \alpha=1,\\<0 & \text{for } \alpha=2.\end{cases} \tag{45}$$

The foregoing grazing conditions are presented in Fig. 9. The vector fields $\mathbf{F}_1^{(1)}(t)$ and $\mathbf{F}_2^{(2)}(t)$ in Ω_1 and Ω_2 are expressed by the dashed and solid arrow-lines, respectively. The force condition in Eq. (44) for the grazing motion in Ω_α is presented through the vector fields of $\mathbf{F}_{\alpha}^{(\alpha)}(t)$. In addition to the necessary condition $F_{\alpha}(\mathbf{x}_m,t_{m\pm})=0$, the sufficient condition requires $F_1(\mathbf{x}_m,\Omega t_{m-\varepsilon})<0$ and $F_1(\mathbf{x}_m,\Omega t_{m+\varepsilon})>0$ in domain Ω_1; and $F_2(\mathbf{x}_m,\Omega t_{m-\varepsilon})>0$ and $F_2(\mathbf{x}_m,\Omega t_{m+\varepsilon})<0$ in domain Ω_2. The detailed investigation of the grazing phenomena can be referred to Luo and Gegg [35].

4. Mapping structures and periodic motions

In this section, the mapping structures for periodic motion will be developed for the friction-induced oscillator. For the constant belt speed, Eq. (3) will hold. Direct integration of Eq. (3) with

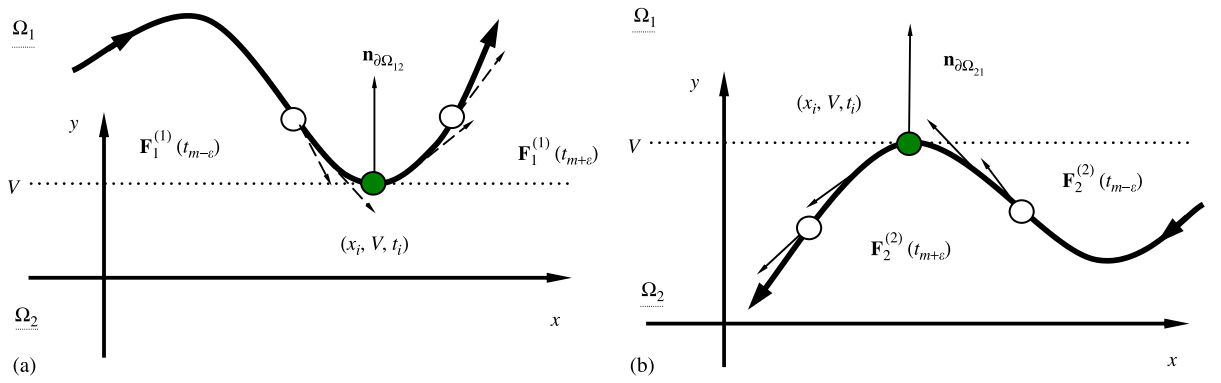

Fig. 9. Vector fields of grazing motions: (a) in Ω_1 and (b) in Ω_2 for the belt speed $V>0$.

initial condition (t_i, x_i, V) yields

$$x = V(t - t_i) + x_i. \tag{46}$$

For the model in Eq. (5), substitution of Eq. (46) into Eq. (33) gives the forces in the very small δ-neighborhood of the stick motion ($\delta \to 0$) in the two domains Ω_α ($\alpha \in \{1, 2\}$) i.e.,

$$F_\alpha(t_{m-}) = -2d_\alpha V - c_\alpha[V(t_{m-} - t_i) + x_i] + A_0 \cos \Omega t_{m-} - b_\alpha. \tag{47}$$

For the non-stick motion, the initial conditions are chosen on the velocity boundary (i.e.,$\dot{x}_i = V$), and the solution of Eq. (5) in all the domains Ω_α is listed in the appendix and the subscript indices (α and j) are identical. For coefficients of those solutions in the appendix, $C_k^{(\alpha)}(x_i, \dot{x}_i, t_i) \triangleq C_k^{(\alpha)}(x_i, t_i)$ for $k = 1, 2$. The basic solutions in the appendix will be used for mapping construction. For non-smooth dynamical systems without the closed-form solutions, the mapping construction can be done only by the numerical integration. To demonstrate the methodology, the firction-induced oscillators with the closed-form solutions will be used. To construct the basic mappings, the switching planes in phase space will be introduced first.

In phase plane, the trajectories in Ω_α, starting and ending at the velocity boundary (i.e., from $\partial\Omega_{\beta\alpha}$ to $\partial\Omega_{\alpha\beta}$), are illustrated in Fig. 10. The starting and ending points for mappings P_α in Ω_α are (x_i,V,t_i) and (x_{i+1},V,t_{i+1}), respectively. The stick mapping is P_0. Define the switching planes as

$$\begin{aligned} \Xi^0 &= \{(x_i, \Omega t_i) | \dot{x}_i(t_i) = V\}, \\ \Xi^+ &= \{(x_i, \Omega t_i) | \dot{x}_i(t_i) = V^+\}, \\ \Xi^- &= \{(x_i, \Omega t_i) | \dot{x}_i(t_i) = V^-\}, \end{aligned} \tag{48}$$

where $V^- = \lim_{\delta_V \to 0}(V - \delta_V)$ and $V^+ = \lim_{\delta_V \to 0}(V + \delta_V)$ for arbitrarily small $\delta_V > 0$. Therefore,

$$P_1 : \Xi^+ \to \Xi^+, \quad P_2 : \Xi^- \to \Xi^-, \quad P_0 : \Xi^0 \to \Xi^0. \tag{49}$$

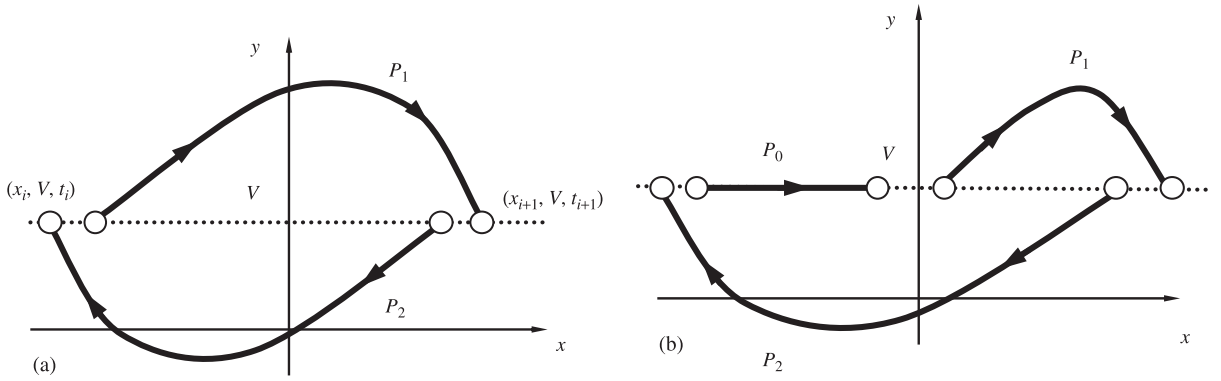

Fig. 10. (a) Regular and (b) stick mappings for oscillators with dry friction.

From the foregoing two equations, we have

$$\begin{aligned} &P_0 : (x_i, V, \Omega t_i) \to (x_{i+1}, V, \Omega t_{i+1}),\\ &P_1 : \left(x_i, V^+, \Omega t_i\right) \to \left(x_{i+1}, V^+, \Omega t_{i+1}\right),\\ &P_2 : (x_i, V^-, \Omega t_i) \to (x_{i+1}, V^-, \Omega t_{i+1}). \end{aligned} \tag{50}$$

The governing equations for P_0 and $\alpha \in \{1, 2\}$ are

$$\begin{aligned} &-x_{i+1} + V(t_{i+1} - t_i) + x_i = 0,\\ &F_\alpha(t_{i+1}) = 0, F_1(t_i) \times F_2(t_i) \leqslant 0. \end{aligned} \tag{51}$$

For the model in Eq. (5), Eq. (51) becomes

$$\begin{aligned} &-x_{i+1} + V(t_{i+1} - t_i) + x_i = 0,\\ &2d_\alpha V + c_\alpha[V(t_{i+1} - t_i) + x_i] - A_0 \cos \Omega t_{i+1} + b_\alpha = 0,\\ &F_1(t_i) \times F_2(t_i) \leqslant 0. \end{aligned} \tag{52}$$

From this problem, the two domains Ω_α ($\alpha \in \{1, 2\}$) are unbounded. The flows of the dynamical systems in the corresponding domains should be bounded from assumptions (A.1)–(A.3). Therefore, only three possible, bounded motions exist in each domains Ω_α ($\alpha \in \{1, 2\}$), from which the governing equations of mapping P_α ($\alpha \in \{1, 2\}$) are obtained. For the non-smooth dynamical systems with the closed-form solutions, the governing equations of each mapping P_λ ($\lambda \in \{0, 1, 2\}$) can be expressed by

$$\begin{aligned} &f_1^{(\alpha)}(x_i, \Omega t_i, x_{i+1}, \Omega t_{i+1}) = 0,\\ &f_2^{(\alpha)}(x_i, \Omega t_i, x_{i+1}, \Omega t_{i+1}) = 0. \end{aligned} \tag{53}$$

Otherwise, such governing equations cannot be obtained analytically. Consider a generalized mapping structure for periodic motion with stick as

$$P = \underbrace{\left(P_2^{(k_{m2})} \circ P_1^{(k_{m1})} \circ P_0^{(k_{m0})}\right) \circ \cdots \circ \left(P_2^{(k_{12})} \circ P_1^{(k_{11})} \circ P_0^{(k_{10})}\right)}_{m-\text{terms}}, \tag{54}$$

where $k_{l\alpha} \in \{0,1\}$ for $l \in \{1,2,\ldots m\}$ and $\lambda \in \{0,1,2\}$. $P_\lambda^{(0)} = 1$ and $P_\lambda^{(k-1)} = P_\lambda \circ P_\lambda^{(k-1)}$. Note that the clockwise and counter-clockwise rotations of the order of the mapping P_λ in the complete mapping P in Eq. (54) will not change the periodic motion. However, the corresponding initial conditions for such a periodic motion are different. For simplicity, the mapping notation in Eq. (53) can be expressed by $P = P_{\underbrace{(2^{k_{m2}}1^{k_{m1}}0^{k_{m0}})\cdots(2^{k_{12}}1^{k_{11}}0^{k_{10}})}_{m\text{-terms}}}$.

For ($m = k_{1,2} = k_{11} = 1$ and $k_{10} = 0$), Eq. (54) gives a mapping structure for the simplest, non-stick periodic motion passing through the separation boundary. The procedure for prediction of periodic motions is presented through this periodic motion. The mapping structure of the simplest periodic motion is

$$P = P_2 \circ P_1 : \Xi^+ \to \Xi^-. \tag{55}$$

From the above relation, we have

$$\begin{aligned} &P_1 : \left(x_i, V^+, t_i\right) \to \left(x_{i+1}, V^+, t_{i+1}\right), \\ &P_2 : (x_{i+1}, V^-, t_{i+1}) \to (x_{i+2}, V^-, t_{i+2}). \end{aligned} \tag{56}$$

Without sliding, $V^+ = V^- = V$ exists. For the periodic motion $\mathbf{y}_{i+2} = P\mathbf{y}_i$ where $\mathbf{y}_i = (x_i, \Omega t_i)^{\mathrm{T}}$ during N-periods of excitation, the periodicity of the periodic motion is

$$x_{i+2} = x_i, \Omega t_{i+2} = \Omega t_i + 2N\pi. \tag{57}$$

For the model in Eq. (5), the governing equations for the simplest periodic motion are

$$\begin{aligned} &f_1^{(1)}(x_i, \Omega t_i, x_{i+1}, \Omega t_{i+1}) = 0, \\ &f_2^{(1)}(x_i, \Omega t_i, x_{i+1}, \Omega t_{i+1}) = 0, \\ &f_1^{(2)}(x_{i+1}, \Omega t_{i+1}, x_{i+2}, \Omega t_{i+2}) = 0, \\ &f_2^{(2)}(x_{i+1}, \Omega t_{i+1}, x_{i+2}, \Omega t_{i+2}) = 0. \end{aligned} \tag{58}$$

With Eq. (57), Eq. (58) gives the initial switching sets for such a periodic motion. The existence of the periodic motion will be determined by the local stability analysis. For the nonlinear, friction-induced oscillators without the closed-form solutions, the numerical algorithm will be used to obtain the initial switching set for such a periodic motion.

Consider the mapping structure for periodic motion with stick ($k = k_{1\alpha} = 1$, $\alpha \in \{0,1,2\}$), the mapping structure for one of the simplest motions with stick is

$$P = P_{210} \triangleq P_2 \circ P_1 \circ P_0. \tag{59}$$

The periodic motion based on the foregoing mapping is sketched in Fig. 11.

For the stick periodic motion $\mathbf{y}_{i+3} = P\mathbf{y}_i$ where $\mathbf{y}_i = (x_i, \Omega t_i)^{\mathrm{T}}$ during N-periods of excitation, the periodicity is

$$x_{i+3} = x_i, \Omega t_{i+3} = \Omega t_i + 2N\pi. \tag{60}$$

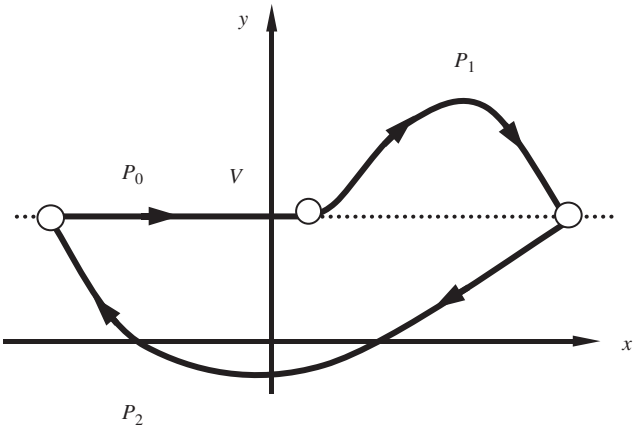

Fig. 11. A periodic motion with stick in oscillators with dry friction.

Again, for the friction-induced oscillators with closed-form solutions, the governing equations for such a periodic motion with stick are

$$f_1^{(\lambda)}(x_{i+\lambda}, \Omega t_{i+\lambda}, x_{i+\lambda+1}, \Omega t_{i+\lambda+1}) = 0,$$
$$f_2^{(\lambda)}(x_{i+\lambda}, \Omega t_{i+\lambda}, x_{i+\lambda+1}, \Omega t_{i+\lambda+1}) = 0 \tag{61}$$

for $\lambda \in \{0, 1, 2\}$. Similarly, the periodic motion for the generalized mapping structure can be predicted through the corresponding governing equations.

To determine the existence of periodic motions, consider the local stability and bifurcation through the eigenvalue analysis based on the corresponding Jacobian matrix. For a periodic motion $\mathbf{y}_{i+\sum_{l=1}^{m}(k_{l2}+k_{l1}+k_{l0})} = P\mathbf{y}_i$, the Jacobian matrix is computed by

$$\mathrm{DP} = \left[\frac{\partial\left(t_{i+\sum_{l=1}^{m}(k_{l2}+k_{l1}+k_{l0})}, x_{i+\sum_{l=1}^{m}(k_{l2}+k_{l1}+k_{l0})}\right)}{\partial(t_i, x_i)}\right]_{(t_i, x_i)}$$
$$= \underbrace{\left(\mathrm{DP}_2^{(k_{m2})} \circ \mathrm{DP}_1^{(k_{m1})} \circ \mathrm{DP}_0^{(k_{m0})}\right) \circ \cdots \circ \left(\mathrm{DP}_2^{(k_{12})} \circ \mathrm{DP}_1^{(k_{11})} \circ \mathrm{DP}_0^{(k_{10})}\right)}_{k-\text{terms}}, \tag{62}$$

where

$$\mathrm{DP}_\lambda = \begin{bmatrix} \dfrac{\partial t_{v+1}}{\partial t_v} & \dfrac{\partial t_{v+1}}{\partial x_v} \\ \dfrac{\partial x_{v+1}}{\partial t_v} & \dfrac{\partial x_{v+1}}{\partial x_v} \end{bmatrix} \tag{63}$$

for $\alpha \in \{0,1,2\}$ and $v \in \{i, i+1, \ldots, i+\sum_{l=1}^{m}(k_{l2}+k_{l1}+k_{l0})-1\}$, and the Jacobian matrix components $\partial t_{v+1}/\partial t_v$, $\partial t_{v+1}/\partial x_v$, $\partial x_{v+1}/\partial t_v$ and $\partial x_{v+1}/\partial x_v$ can be computed through Eqs. (52) and (53). Suppose the eigenvalues for the mapping structure of periodic motion are $\lambda_{1,2}$. The stable period-1 motion requires the eigenvalues be $|\lambda_\alpha|<1$ ($\alpha \in \{1,2\}$). Once the foregoing condition is not satisfied, the period-1 motion is unstable. If $|\lambda_{1or2}| = 1$ with complex numbers, the Neimark bifurcation occurs. If one of the two eigenvalues is -1 (i.e., $\lambda_{1(or\ 2)} = -1$) and the other one is inside the unit circle, the period-doubling bifurcation occurs, i.e.,

$$\mathrm{Det}(\mathrm{DP}) + \mathrm{Tr}(\mathrm{DP}) + 1 = 0. \tag{64}$$

If one of the two eigenvalues is $+1$ (i.e., $\lambda_{1(or\ 2)} = +1$) and the second one is inside the unit circle, the first saddle-node bifurcation occurs, i.e.,

$$\mathrm{Det}(\mathrm{DP}) + 1 = \mathrm{Tr}(\mathrm{DP}). \tag{65}$$

Without the local bifurcation relative to the discontinuity, the eigenvalue analysis can provide an adequate prediction. However, the eigenvalue analysis cannot work for the local bifurcations pertaining to the separation discontinuity. According to the aforementioned causes, the onset, existence and disappearance of the stick motion should be determined through the force criteria in Eqs. (39) and (40). The grazing bifurcation will be determined by Eq. (45). For the general case of the friction-induced oscillators, the eigenvalue analysis cannot be done. However, the force criteria can be embedded in the numerical algorithm to detect the switch, non-stick and grazing motions.

5. Illustrations

Consider the system parameters ($V = 1$, $A_0 = 90$, $d_1 = 1$, $d_2 = 0$, $b_1 = -b_2 = 30$, $c_1 = c_2 = 30$), as an example for illustration. The *numerical* prediction of a bifurcation scenario on switching phase and displacement varying with excitation frequency is illustrated in Fig. 12. All the numerical computations are completed from the closed-form solutions in the appendix. Based on the methodology presented in this paper, the straight-forwarded numerical integration with the appropriate accuracy can be also used for numerical predictions of nonlinear, non-smooth dynamical systems. The dashed and dash-dot vertical lines denote the boundaries for the onset and vanishing of sliding motion (or stick motion) and for grazing bifurcation, respectively. The acronyms "SB" and "GB" individually represent the *sliding* and *grazing* bifurcations. The regions between two adjacent boundary lines are labeled with corresponding mapping structures for $\Omega \in (0.333, 90.330)$. If the excitation frequency is either less than the lowest boundary or greater than the highest boundary, no periodic motion intersects with the separation boundary $y = V$ (i.e., $V = 1$). The periodic motion for P_{20} is in range of $\Omega \in (80.215, 90.330)$. The periodic motion for P_{201} is in range of $\Omega \in (52.600, 80.214)$ and $(2.397, 3.539)$. The periodic motion for P_{21} is in the range of $\Omega \in (3.540, 52.599)$. The periodic motion for $P_{2(01)^2}$ is in the range of $\Omega \in (2.372, 2.396)$. The periodic motion for P_{0201} is in the range of $\Omega \in (1.669, 2.371)$, $(0.974, 1.159)$ and $(0.726, 0.748)$. The periodic motion for $P_{(02)^2 01}$ is in the range of $\Omega \in (1.160, 1.669)$, $(0.749, 0.973)$ and $(0.629, 0.725)$. The periodic motion for $P_{(20)^2}$ is in range of $\Omega \in (0.610, 0.628)$ and $(0.543, 0.588)$. The periodic motion for $P_{(20)^3}$ is in the range of $\Omega \in (0.599, 0.609)$ and $(0.536, 0.542)$. Finally, the

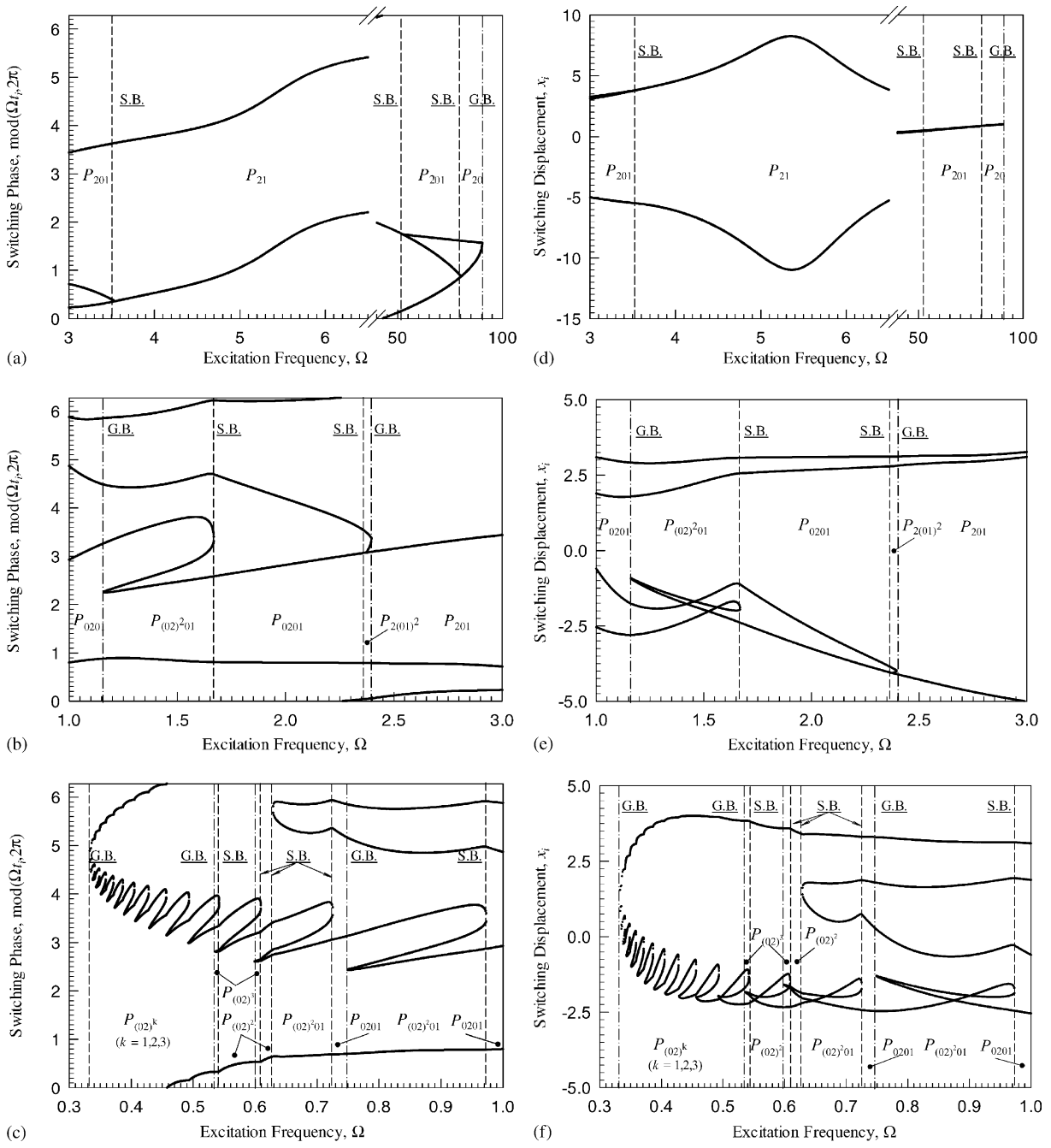

Fig. 12. The *numerical* prediction of bifurcation diagram: (a)–(c) switching phase and (d)–(f) switching displacement varying with excitation frequency ($V = 1$, $A_0 = 90$, $d_1 = 1$, $d_2 = 0$, $b_1 = -b_2 = 30$, $c_1 = c_2 = 30$). The dashed and dash-dot, vertical lines denote the boundaries for the onset and vanishing of sliding motion, and for grazing bifurcation, respectively.

Table 1
The summary of excitation frequencies for specific motions ($V = 1$, $A_0 = 90$, $d_1 = 1$, $d_2 = 0$, $b_1 = -b_2 = 30$, $c_1 = c_2 = 30$)

Mapping structures	Excitation frequency	Grazing bifurcation	Sliding bifurcation
P_{20}	(80.215,90.330)	90.33	80.214–80.215
P_{201}	(52.600,80.214) (2.397,3.539)	2.396–2.397	80.214–80.215 52.599–52.600 3.539–3.540
P_{21}	(3.540,52.599)	—	52.599–52.600 3.539–3.540
$P_{2(01)^2}$	(2.372,2.96)	2.396–2.397	2.371–2.372
P_{0201}	(1.670,2.371) (0.974,1.159) (0.726,0.748)	0.748–0.749 1.159–1.160	2.371–2.372 1.669–1.670 0.973–0.974 0.725–0.725
$P_{(02)^2 01}$	(1.160,1.669) (0.749,0.973) (0.629,0.725)	1.159–1.160 0.748–0.749	1.669–1.670 0.973–0.974 0.725–0.725 0.628–0.629
$P_{(20)^2}$	(0.610,0.628) (0.543,0.598)	0.598–0.599 0.542–0.543	0.628–0.629 0.609–0.610
$P_{(20)^3}$	(0.599,0.609) (0.536,0.542)	0.598–0.599 0.535–0.536	0.609–0.610 0.542–0.543
$P_{(20)^k}$ $(k = 1, 2, 3)$	(0.333,0.535)	—	—

periodic motion for $P_{(20)^k}$ $(k = 1, 2, 3, \ldots)$ is in range of $\Omega \in (0.333, 0.535)$. The grazing bifurcation occurs at the following approximate excitation frequencies $\{90.330, 2.397, 1.160, 0.749, 0.542, \ldots\}$. For $\Omega \approx 2.397$, the grazing bifurcation for mapping P_1 exists, and the other critical values are for the grazing bifurcations of mapping P_2. The onset and vanishing of stick periodic motions occur at the approximate excitation frequencies $\{80.214, 52.600, 3.540, 2.371, 1.669, 0.973, 0.725, 0.629, 0.610, 0.599, 0.543\}$. Excitation frequencies for specific periodic motions, grazing and sliding bifurcations are summarized in Table 1 with parameters ($V = 1$, $A_0 = 90$, $d_1 = 1$, $d_2 = 0$, $b_1 = -b_2 = 30$, $c_1 = c_2 = 30$).

Using the mapping structure in Eq. (54), all the periodic motions for the entire range of excitation frequency can be determined analytically by the corresponding governing equations similar to Eqs. (60) and (61). The mapping structure gives the nonlinear algebraic equations, solved by the Newton–Raphson method. To make the computation convergent fast, the initial guess solutions should be chosen in the appropriate convergent domain. Once the first solution is obtained, the rest solutions with varying parameters can be determined through the corresponding

mapping structure. The same parameters as in the numerical analysis are adopted. The analytical prediction of the stick and non-stick periodic motions is given for $\Omega \in (0.536, 90.333)$, and the switching phase and switching displacements of the periodic motions are plotted in Fig. 13. As in Fig. 12, the dashed and dash-dot vertical lines denote the boundaries for the onset and vanishing of stick motions and for grazing bifurcation, respectively. The regions between two adjacent boundary lines are labeled with corresponding mapping structures. In addition, the switching phases and displacements are also labeled for the corresponding mapping. The intersected points between the switching phases/displacements and the vertical boundary lines are marked by the hollow circular symbols. It is observed that this *analytical* prediction of the periodic motions is identical to the *numerical* prediction as presented previously. For nonlinear, non-smooth dynamical systems, the analytical predictions cannot be carried out. The numerical algorithms with the force criteria will be used for numerical predictions. However, the numerical predictions give only one branch of multiple solutions of non-smooth dynamical systems. To get the rest solutions, the symmetry of solutions should be considered by use of the corresponding the mapping structure. The detailed discussion for the symmetry of periodic motions in non-smooth dynamical systems can be referred to Luo [36].

The eigenvalue analysis of the analytical solutions based on the mapping structure can be completed very easily according to the procedure presented in Section 4. The magnitude and real parts of eigenvalues for all the analytical solutions of periodic motions are illustrated in Fig. 14(a)–(c) and (d)–(f), respectively. The corresponding mapping structures are labeled as in Figs. 12 and 13. From the local stability analysis of the periodic motions, all the periodic motions are always stable before a new periodic motion appears. Therefore, the traditional eigenvalue analysis tells us that those periodic motions may exist in the wide range of parameters. However, before the local stability conditions are destroyed, the existing periodic motion already switches to a new periodic motion due to a global event, resulting from the stick and grazing bifurcations. Once the stick motion exists, the traditional eigenvalue analysis for the motion switching cannot work well. In Fig. 14, it is clearly seen that, from the non-stick motion to the stick motion, one of the eigenvalues for the periodic motion is zero. From a stick motion to an adjacent stick motion, the eigenvalue analysis cannot provide further information to find any signature of the motion switching.

Using the mapping structures and the criteria for stick motions in Eqs. (38)–(40), the regions of periodic motions in parameter space are illustrated in Fig. 15 through excitation amplitude and frequency with the prescribed parameters ($V = 1$, $A_0 = 90$, $d_1 = 1$, $d_2 = 0$, $b_1 = -b_2 = 30$, $c_1 = c_2 = 30$). The acronym "NM" denotes no periodic motion intersecting with the separation boundary (i.e., $y = V$). The regions of periodic motions in parameter space (Ω, A_0) are plotted in Fig. 15(a) under the prescribed parameters. The detailed view of periodic motion for small excitation frequencies is given in Fig. 15(b). With increasing excitation amplitude, the periodic motion with mapping structure P_{21} possesses a wider range of excitation frequency. However, the range of excitation frequency for stick motion becomes smaller, and the mapping structures for stick motions become much simpler. To consider the effects of the friction force, the regions of periodic motions is formed through friction force and excitation frequency, as shown in Fig. 16 for the parameters ($V = 1$, $A_0 = 90$, $d_1 = 1$, $d_2 = 0$, $b_1 = -b_2 = 30$, $c_1 = c_2 = 30$). With increasing friction force, the range of excitation frequency for the non-stick motion becomes smaller and smaller;

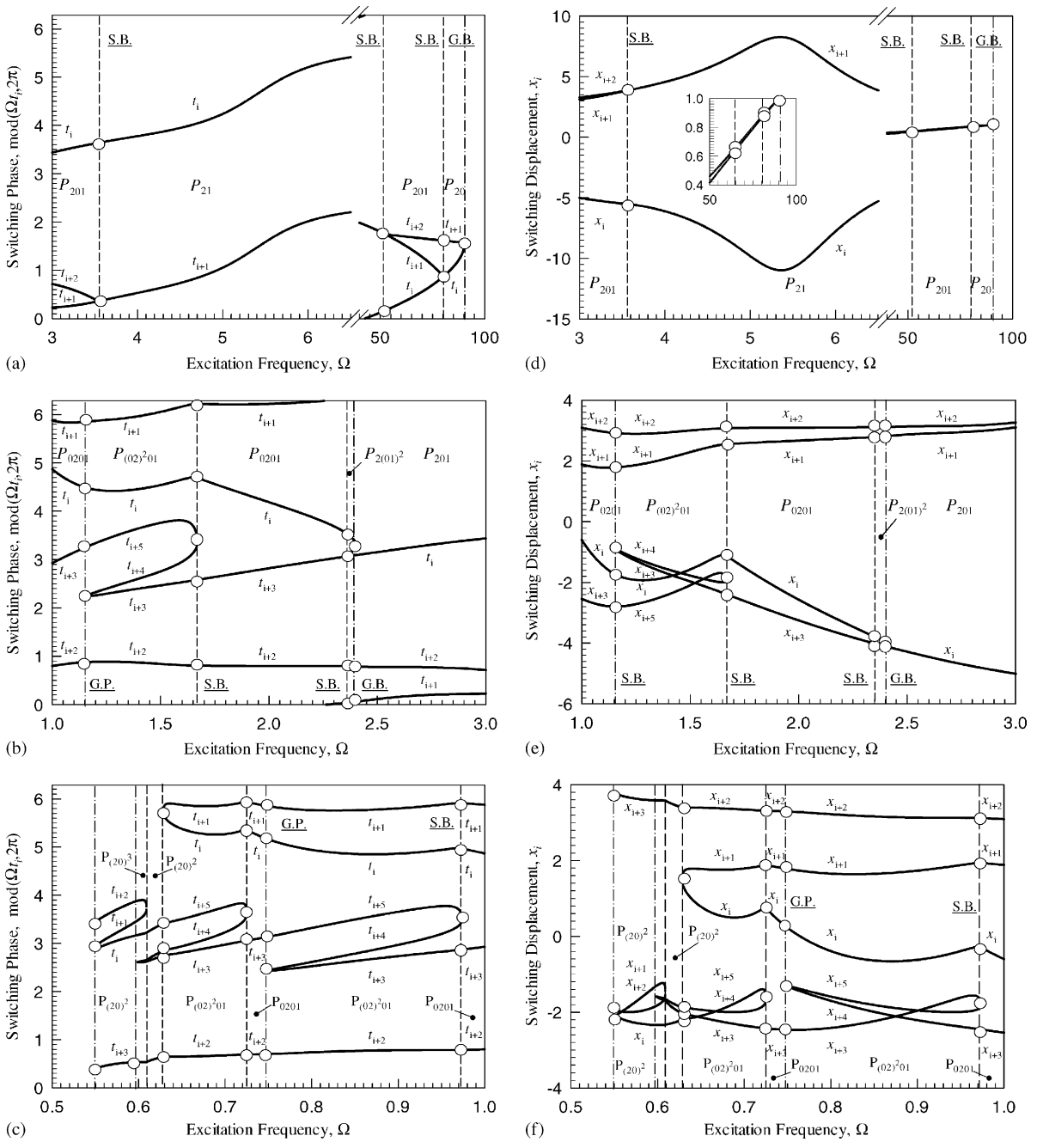

Fig. 13. The *analytical* prediction of periodic motions: (a)–(c) switching phase and (d)–(f) switching displacement varying with excitation frequency ($V = 1$, $A_0 = 90$, $d_1 = 1$, $d_2 = 0$, $b_1 = -b_2 = 30$, $c_1 = c_2 = 30$). The dashed and dash-dot, vertical lines denote the boundaries for the onset and vanishing of sliding motion, and for grazing bifurcation, respectively.

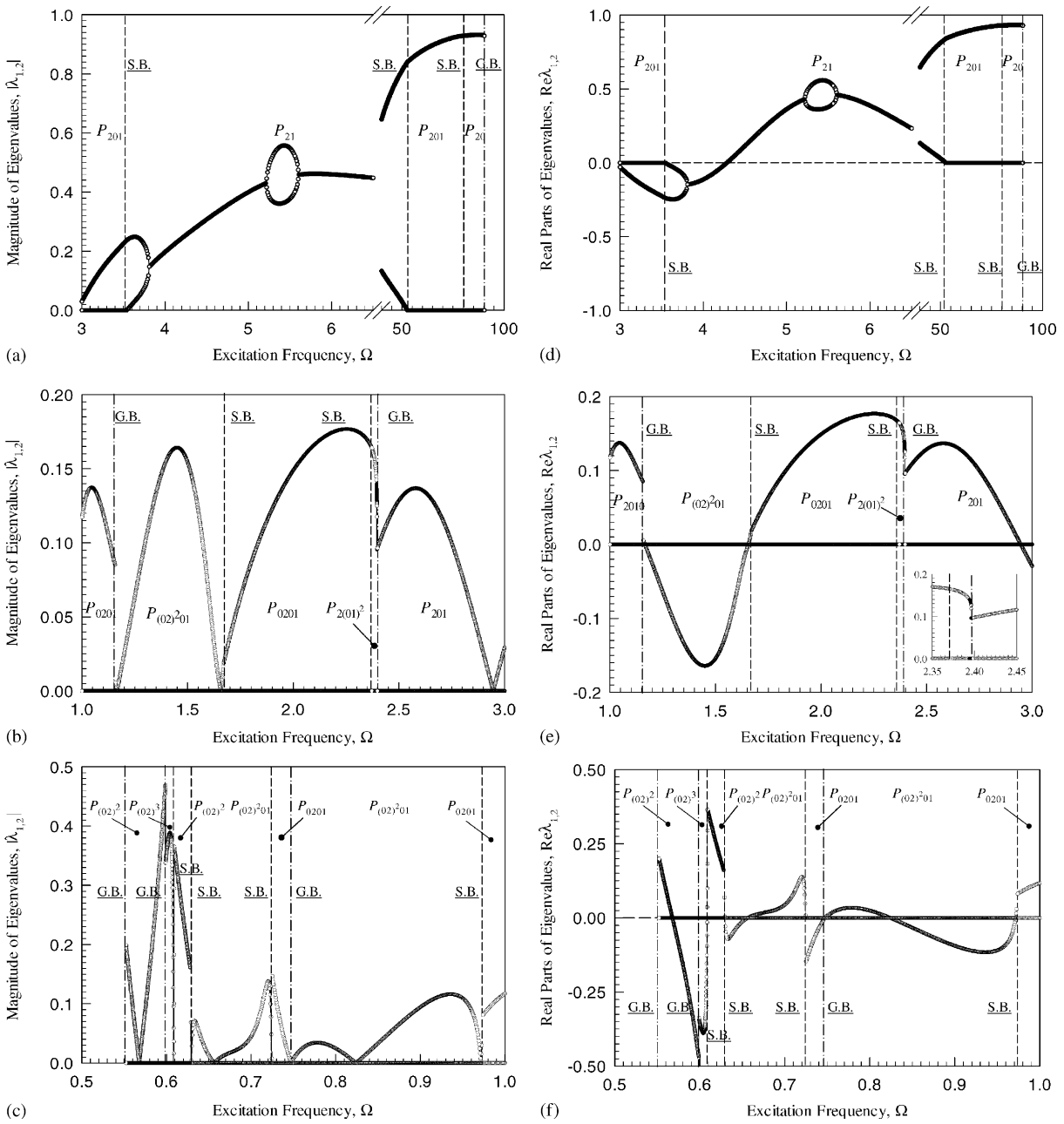

Fig. 14. The *eigenvalue analysis* of periodic motions: (a)–(c) magnitudes (d)–(f) real parts of eigenvalues varying with excitation frequency ($V = 1$, $A_0 = 90$, $d_1 = 1$, $d_2 = 0$, $b_1 = -b_2 = 30$, $c_1 = c_2 = 30$). The dashed and dash-dot, vertical lines denote the boundaries for the onset and vanishing of sliding motion, and for grazing bifurcation, respectively.

and the motion relative to P_1 will finally disappear. With further increasing the friction forces, only the stick motion with mapping structures $P_{(20)^k}$ ($k = 1, 2, 3, \ldots$) exists. However, the stick motions for smaller friction forces will be more complicated than for larger fiction forces.

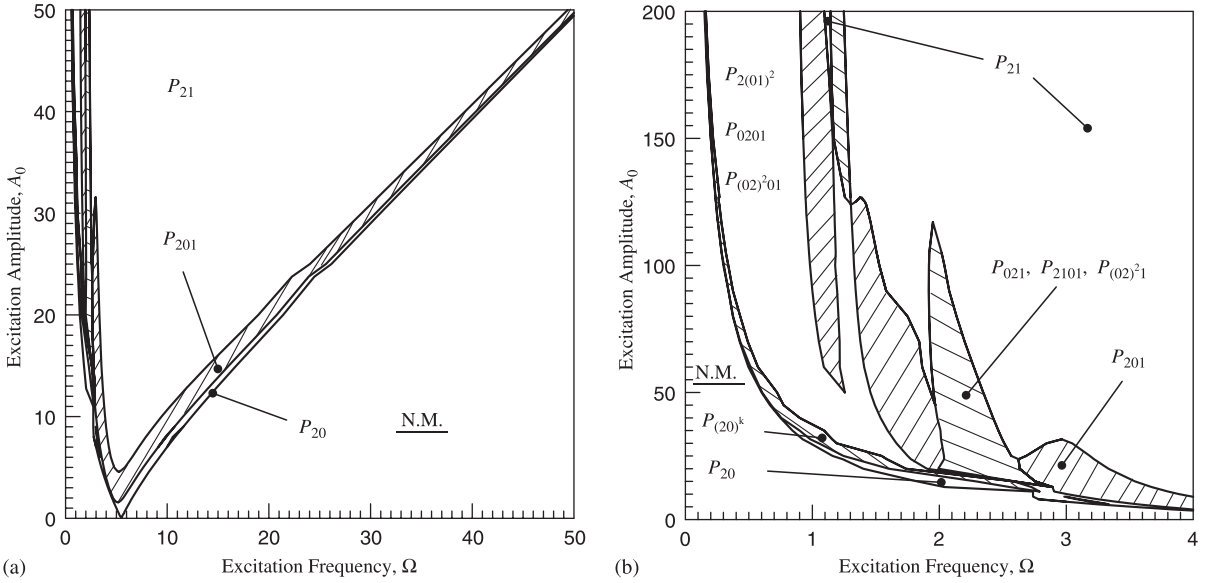

Fig. 15. The regions of periodic motions in parameter space: (a) excitation amplitude versus frequency and (b) a detailed view for small excitation frequencies ($V = 1$, $d_1 = 1$, $d_2 = 0$, $b_1 = -b_2 = 30$, $c_1 = c_2 = 30$). The acronym "NM" represents the region for non-motion intersected with the separation boundary.

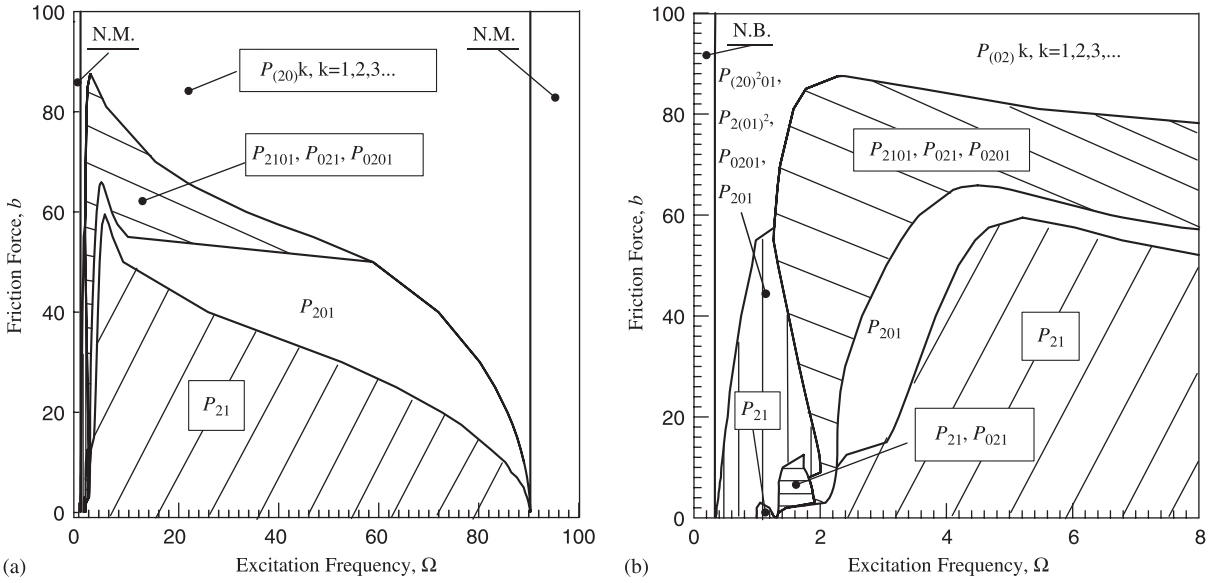

Fig. 16. The regions of periodic motions in parameter space: (a) friction force versus excitation frequency and (b) a detailed view for small excitation frequencies ($V = 1$, $A_0 = 90$, $d_1 = 1$, $d_2 = 0$, $b_1 = -b_2 = b$, $c_1 = c_2 = 30$). The acronym "NM" represents the region for non-motion intersected with the separation boundary.

6. Simulations

The motion parametric characteristics of the oscillator with dry friction in parameter space have been systematically investigated. To verify the analytical prediction of the periodic motions, the periodic motions in the oscillator will be demonstrated through time-history responses and phase space. From the analytical investigation, it is found that the force responses play an important role in discontinuous dynamical systems. Therefore, the force responses will be presented to illustrate the criteria for the onset and vanishing of stick motions in such a friction-induced oscillator. In addition, the mechanism of stick and non-stick motions in friction-induced oscillators will be further discussed. The input data for numerical simulations are tabulated in Table 2.

Consider the parameters (i.e., $V = 1$, $A_0 = 90$, $d_1 = 1$, $d_2 = 0$, $b_1 = -b_2 = 30$, $c_1 = c_2 = 30$) for illustrations. Phase trajectories for several specific mapping structures are demonstrated in Figs. 17 and18. The dark circular symbols represent the passable motion flow from domain Ω_α to Ω_β, $\{\alpha, \beta\} \in \{1, 2\}$ and $\alpha \neq \beta$. The gray and hollow circular symbols represent the onset and vanishing of the stick motion along the separation boundary, respectively. The shaded areas in phase planes are relative to the regions of stick motions. In Fig. 17, trajectories in phase planes are arranged in Fig. 17(a)–(d), respectively, for the stick, periodic motions with mapping structures P_{201}, P_{2010}, $P_{(02)^2 01}$ and $P_{(20)^2}$. Each segment of the trajectory in phase plane, corresponding to the specific mapping, is also labeled. The different, stick periodic motions possess completely different orbits in the phase plane. The trajectory of the mapping $P_{(02)^2 01}$ is very interesting because of the combination of the stick and non-stick motions. To further observe the complexity of the trajectories relative to mapping $P_{(02)^2 01}$, more phase trajectories for such a periodic motion are plotted in Fig. 18(a) and (b). The periodic motions relative to mapping P_{0201} and very close to P_{22010} are also presented in Fig. 18(c) and (d) to explain the motion transition from P_{0201} to

Table 2
Input data for numerical simulations ($V = 1$, $d_1 = 1$, $d_2 = 0$, $b_1 = -b_2 = b$, $c_1 = c_2 = 30$)

	Friction b	Excitation (Ω, A_0)	Initial conditions $(x_i, y_i, \Omega t_i)$	Mapping structures
Fig. 17	30	(70.0, 90)	(0.7151659580,1.0,0.5549996200)	$\underline{P_{201}}$
	30	(1.75,90)	(−2.617341234,1.0,2.639329565)	$\underline{P_{2010}}$(or $\underline{P_{0201}}$)
	30	(1.35, 90)	(−1.891740094,1.0,4.433773820)	$\underline{P_{(02)^2 01}}$
	30	(0.52, 90)	(−2.237163685,1.0,3.212714000)	$\underline{P_{(20)^2}}$
Fig. 18	30	(0.7, 90)	(0.5175912680,1.0,5.268734020)	$\underline{P_{(02)^2 01}}$
	30	(0.9, 90)	(−0.6199800230,1.0,4.861840257)	$\underline{P_{(02)^2 01}}$
	30	(1.1, 90)	(−2.763943025,1.0,3.146400000)	$\underline{P_{0201}}$
	30	(1.16, 90)	(−2.806638239,1.0,3.812031430)	$\underline{P_{22010}}$(or $\underline{P_{02201}}$)
Fig. 19	30	(4, 90)	(−6.112684135,1.0,3.776978988)	$\underline{P_{21}}$
Fig. 20	3	(2.74,15)	(−0.8285986540,1.0,3.176648200)	$\underline{P_{2(01)^2}}$
Fig. 21	3	(2.58,23.25)	(−1.071028626,1.0,3.055083416)	$\underline{P_{2101}}$
Fig. 22	30	(1.49, 90)	(−1.947416143,1.0,2.459350054)	$\underline{P_{201020}}$

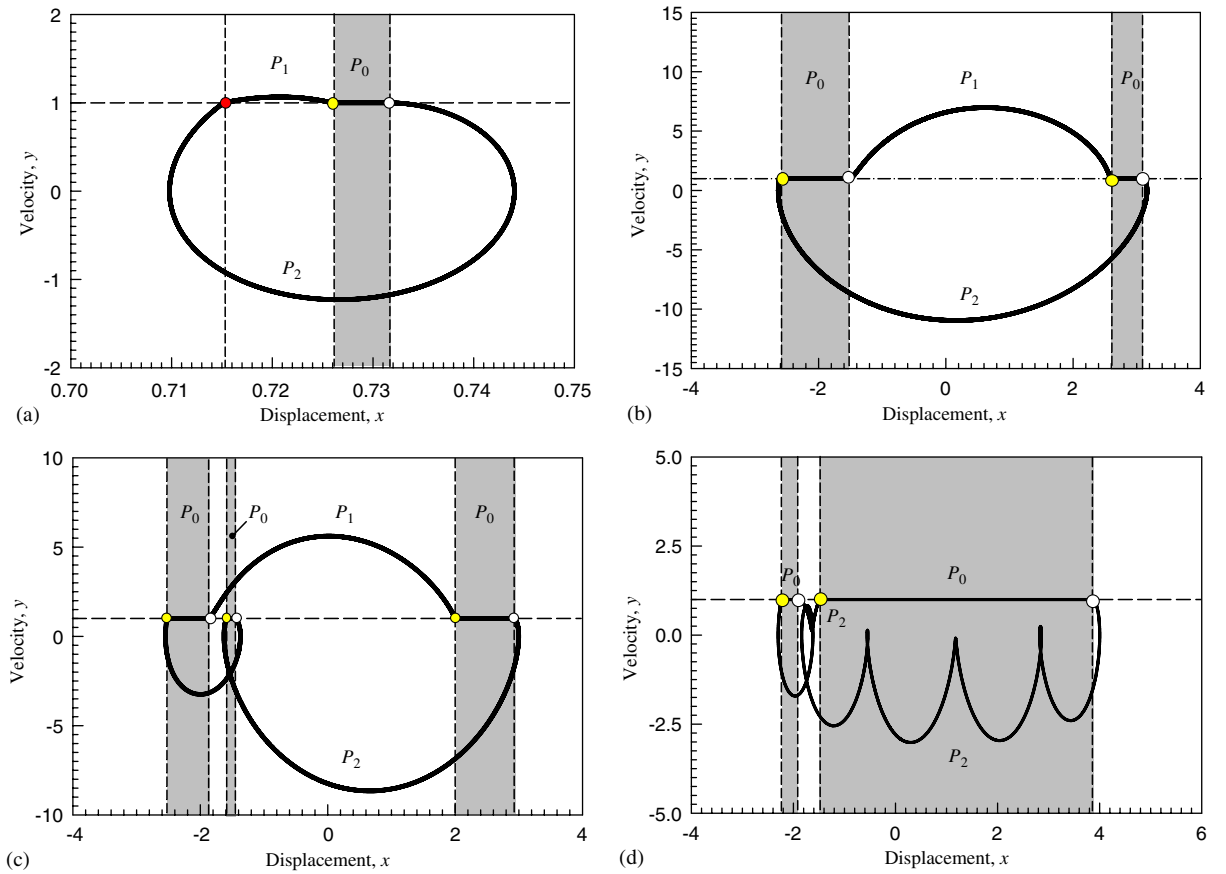

Fig. 17. Phase trajectories for stick, periodic motions ($V = 1$, $A_0 = 90$, $d_1 = 1$, $d_2 = 0$, $b_1 = -b_2 = 30$, $c_1 = c_2 = 30$, $y_i = V$): (a) P_{201} ($\Omega = 70$, $x_i \approx 0.7151659580$, $\Omega t_i \approx 0.5549996200$); (b) P_{2010} (or P_{0201}) ($\Omega = 1.75$, $x_i \approx -2.617341234$, $\Omega t_i \approx 2.639329565$); (c) $P_{(02)^2 01}$ ($\Omega = 1.35$, $x_i \approx -1.8917400940$, $\Omega t_i \approx 4.433773820$); (d) $P_{(20)^2}$ (or$P_{(02)^2}$) ($\Omega = 0.52$, $x_i \approx -2.37163685$, $\Omega t_i \approx 3.212714000$). The dark circular symbols represent the passable motion from domain Ω_α to Ω_β, $\{\alpha, \beta\} \in \{1, 2\}$ and $\alpha \neq \beta$. . The gray and hollow circular symbols represent the onset and vanishing of stick motion along the separation boundary, respectively.

$P_{(02)^2 01}$. The trajectory of the stick periodic motion in Fig. 18(d) is very close to grazing motion of P_{22010}. After the grazing motion relative to P_{0201}, the periodic motions pertaining to mapping $P_{(02)^2 01}$ will occur.

The dynamical forces are very important to predict stick motions. For a better understanding of the mechanism of stick motion, the time-history responses for displacement, velocity, and forces will be illustrated, and the relationships between the displacement/velocity and the force will be presented. The responses of the non-stick periodic motion of mapping P_{21} are plotted in Fig. 19. No stick motion (or sliding motion) exists on the separation boundary in Fig. 19(a). The mapping switching from P_α to P_β $\{\alpha, \beta\} \in \{1, 2\}$ and $\alpha \neq \beta$) is continuous without stick. The relation between the displacement and force in Fig. 19(b) verifies the criteria in the second equation of Eq. (38) at the velocity separation boundary. Namely, the signs of two forces on the boundary are same,

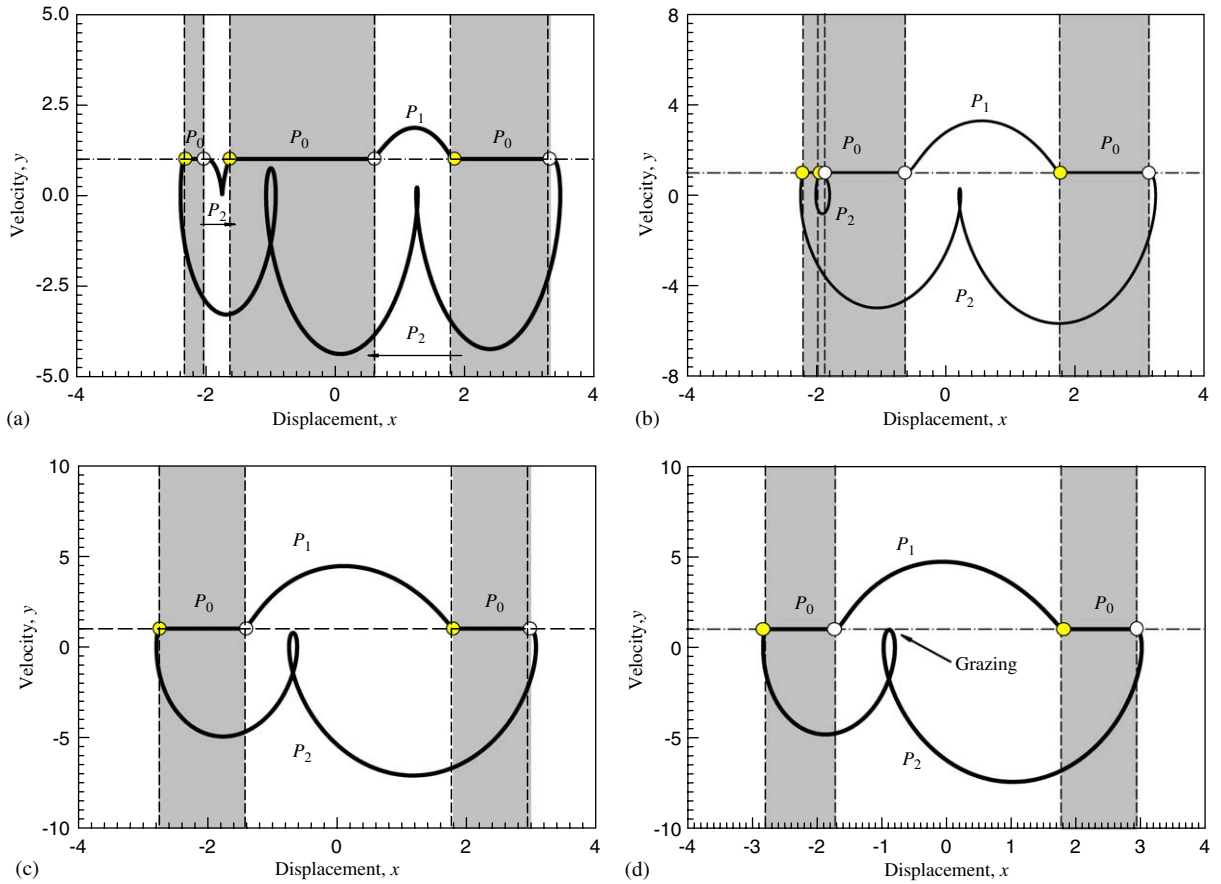

Fig. 18. Phase trajectories for stick periodic motions ($V = 1$, $A_0 = 90$, $d_1 = 1$, $d_2 = 0$, $b_1 = -b_2 = 30$, $c_1 = c_2 = 30$, $y_i = V$): (a) $P_{(02)^2 01}$ ($\Omega = 0.7$, $x_i \approx 0.5175912680$, $\Omega t_i \approx 5.268734026$); (b) $P_{(02)^2 01}$ ($\Omega = 0.9$, $x_i \approx -0.6199800230$, $\Omega t_i \approx 4.861840257$); (c) P_{0201} ($\Omega = 1.1$, $x_i \approx -2.7639430250$, $\Omega t_i \approx 3.146400000$); (d) P_{22010} (orP_{02201}) ($\Omega = 1.15$, $x_i \approx -2.806638239$, $\Omega t_i \approx 3.812031430$). The dark circular symbols represent the passable motion from domain Ω_α to Ω_β, $\{\alpha, \beta\} \in \{1, 2\}$ and $\alpha \neq \beta$. The gray and hollow circular symbols represent the onset and vanishing of stick motion along the separation boundary, respectively.

which is also clearly shown in Fig. 19(c) through the dynamical forces and velocity. The time-history responses of displacement, velocity, and forces are shown in Fig. 18(d)–(f), respectively. The switching points are marked by the dark circular symbols. The vertical, dashed lines are the separation boundary lines, which imply the motion switching. The corresponding mappings are labeled in plots of displacement and velocity responses.

To compare with the above non-stick motion, stick motions for such a friction-induced oscillator are presented in Figs. 20–22 for mapping structures $P_{2(01)^2}$, P_{2101} and P_{201020} (or $P_{(02)^2 01}$) accordingly. The motions of $P_{2(01)^2}$ and P_{2101} cannot be observed for $A_0 = 90$. Therefore, the different excitations and friction forces are used to demonstrate such periodic motions. The transition from P_{2101} to $P_{2(01)^2}$ is caused by a grazing of mapping P_1. The responses of periodic

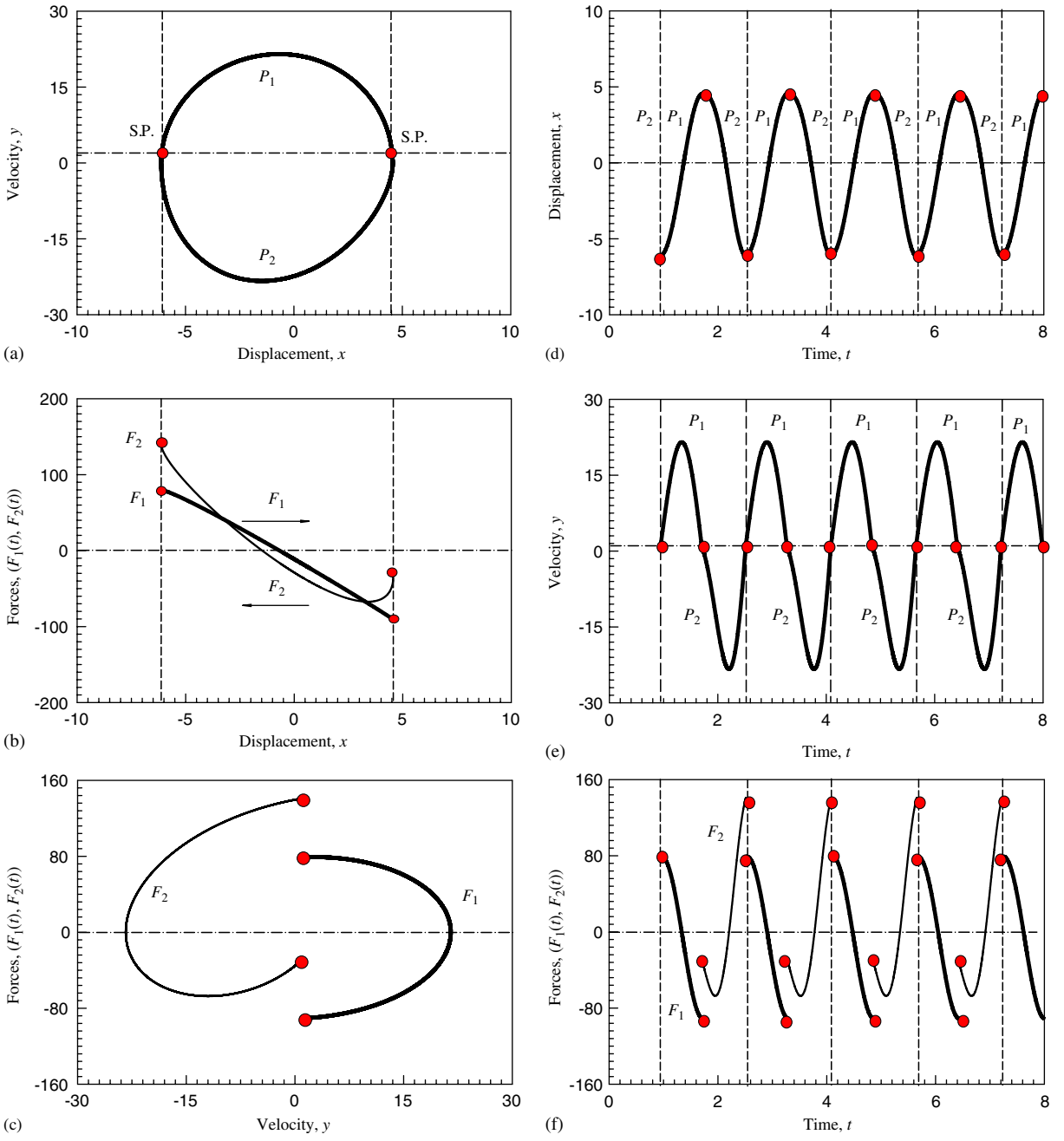

Fig. 19. Displacement, velocity and force responses of *non-stick*, periodic motion with P_{21} for $\Omega = 4$ and the initial conditions $(x_i \approx -6.112684135, \Omega t_i \approx 3.776978988, y_i = V)$ $(V = 1, A_0 = 90, d_1 = 1, d_2 = 0, b_1 = -b_2 = 30, c_1 = c_2 = 30)$. The dark symbol represents the passable motion from domain Ω_α to Ω_β, $\{\alpha, \beta\} \in \{1, 2\}$ and $\alpha \neq \beta$. The gray and hollow circular symbols represent the onset and vanishing of stick motion along the separation boundary, respectively.

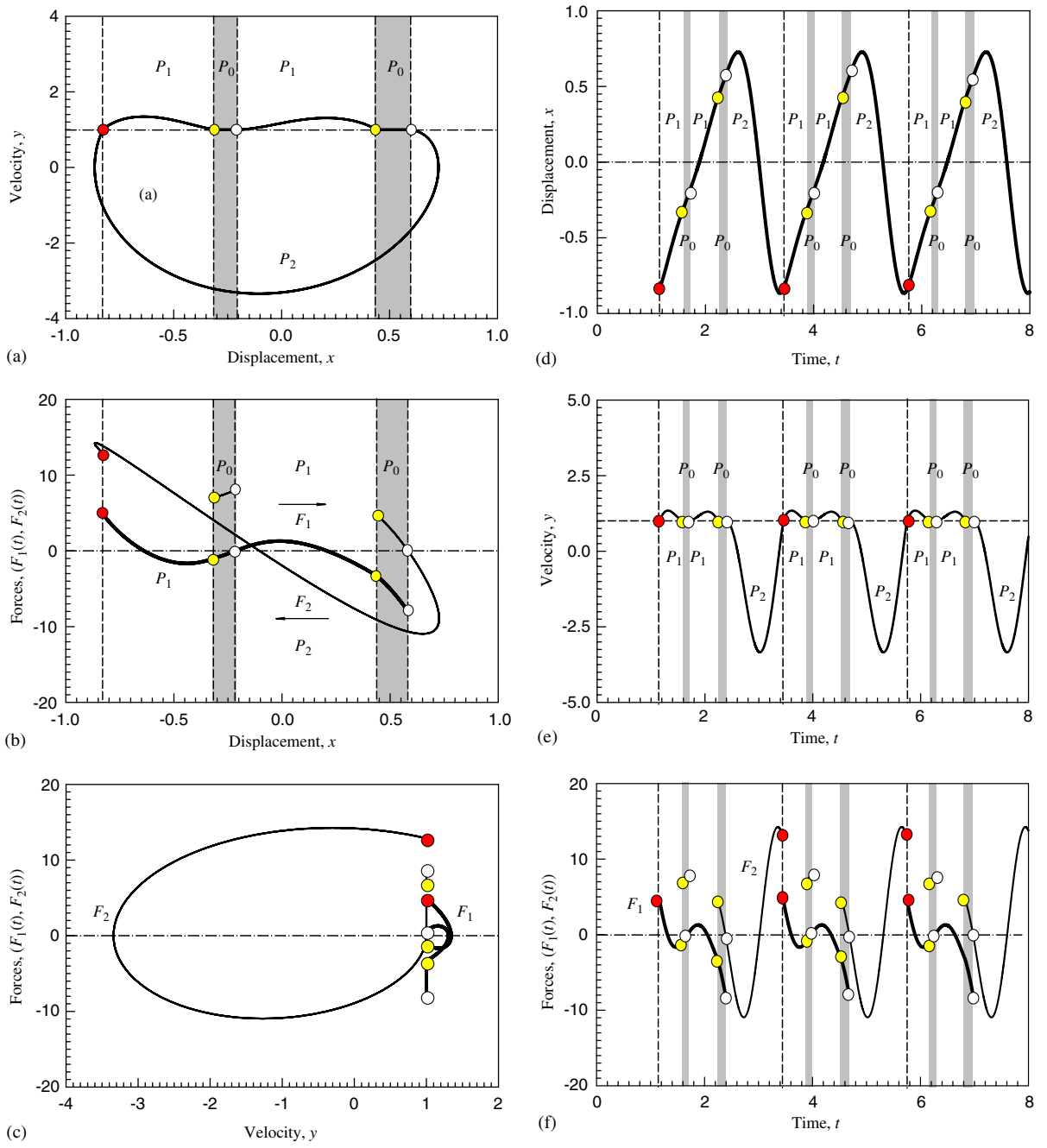

Fig. 20. Displacement, velocity and force responses of *stick*, periodic motion with $P_{2(01)^2}$ for $\Omega = 2.74$ and the initial conditions ($x_i \approx -0.8285985640$, $\Omega t_i \approx 3.1766482$, $y_i = V$) ($V = 1$, $A_0 = 15$, $d_1 = 1$, $d_2 = 0$, $b_1 = -b_2 = 3$, $c_1 = c_2 = 30$). The dark symbol represents the passable motion from domain Ω_α to Ω_β, $\{\alpha, \beta\} \in \{1, 2\}$ and $\alpha \neq \beta$. The gray and hollow circular symbols represent the onset and vanishing of stick motion along the separation boundary, respectively.

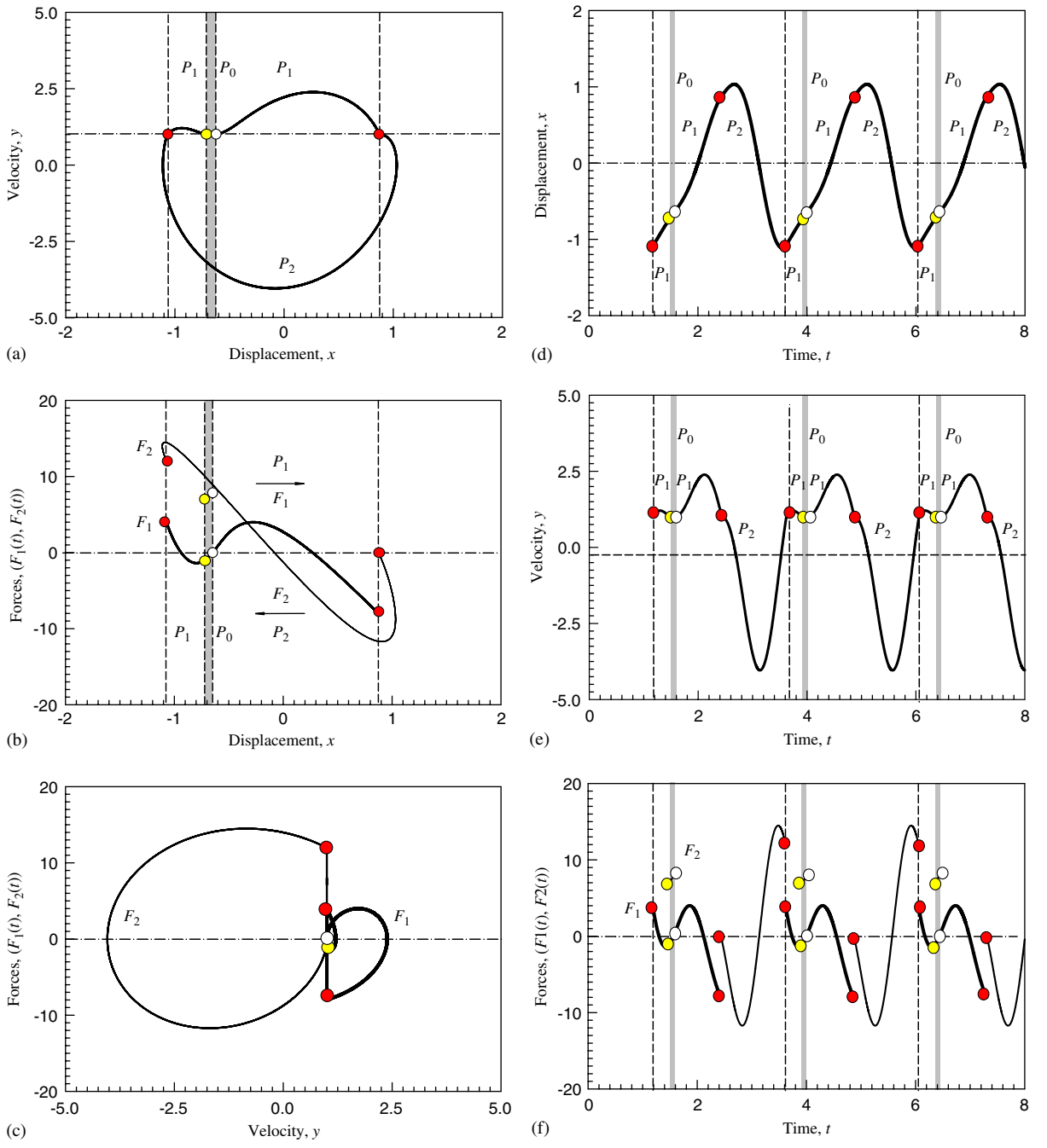

Fig. 21. Displacement, velocity and force responses of *stick*, periodic motion with $\boldsymbol{P}_{2101}$ for $\Omega = 2.58$ and the initial conditions ($x_i \approx -1.0710286260$, $\Omega t_i \approx 3.055083416$, $y_i = V$) ($V = 1$, $A_0 = 23.25$, $d_1 = 1$, $d_2 = 0$, $b_1 = -b_2 = 3$, $c_1 = c_2 = 30$). The dark symbol represents the passable motion from domain Ω_α to Ω_β, $\{\alpha, \beta\} \in \{1, 2\}$ and $\alpha \neq \beta$. The gray and hollow circular symbols represent the onset and vanishing of stick motion along the separation boundary, respectively.

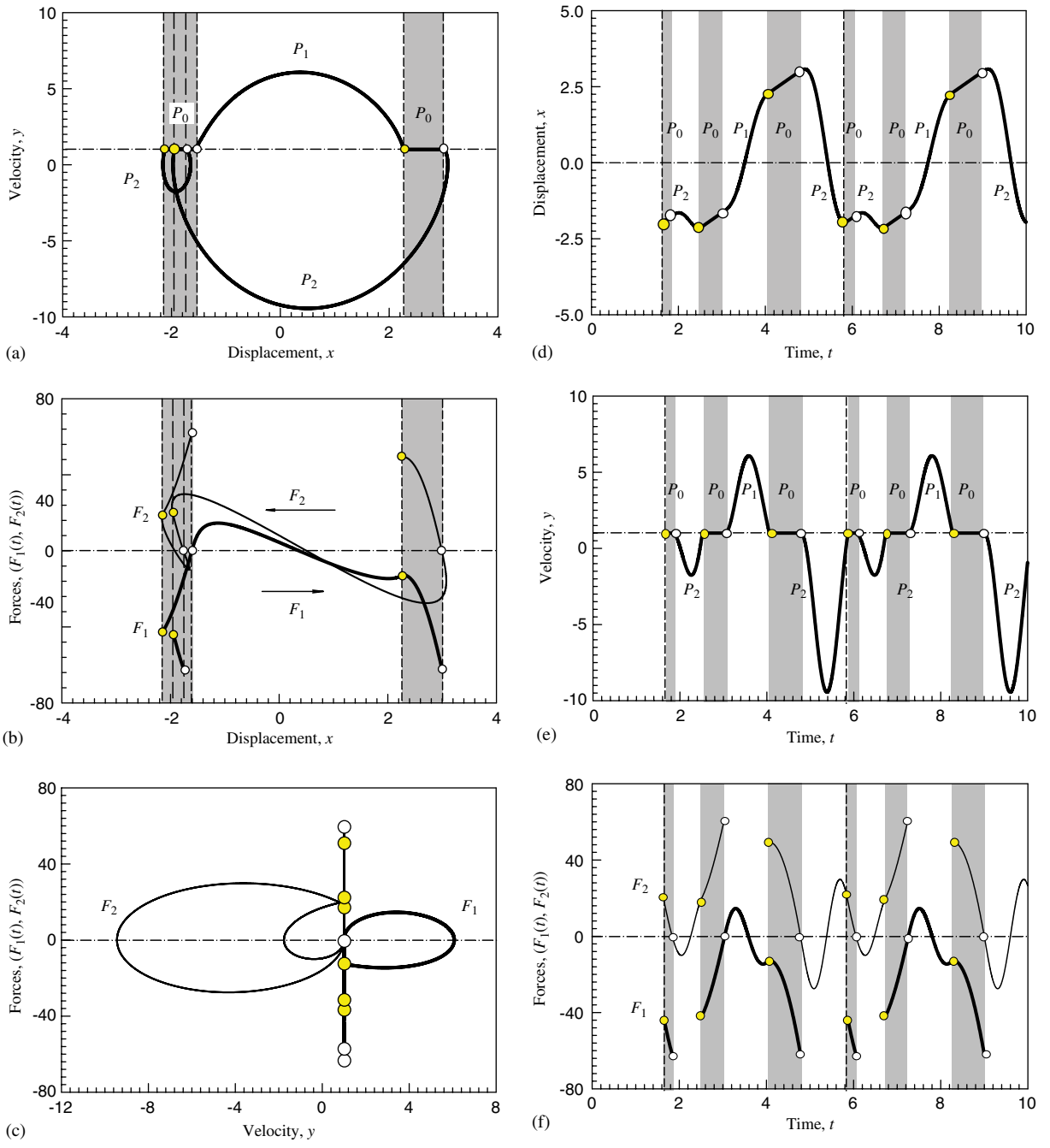

Fig. 22. Displacement, velocity and force responses of *stick*, periodic motion with $\boldsymbol{P}_{201020}$ (or $P_{(02)^2 01}$) for $\Omega = 1.49$ and the initial conditions ($x_i \approx -1.9474161430$, $\Omega t_i \approx 2.459350054$, $y_i = V$) ($V = 1$, $A_0 = 90$, $d_1 = 1$, $d_2 = 0$, $b_1 = -b_2 = 30$, $c_1 = c_2 = 30$). The dark symbol represents the passable motion from domain Ω_α to Ω_β, $\{\alpha, \beta\} \in \{1, 2\}$ and $\alpha \neq \beta$. The gray and hollow circular symbols represent the onset and vanishing of stick motion along the separation boundary, respectively.

motions pertaining to $P_{2(01)^2}$ are presented in Fig. 20. Two stick parts exist in this periodic motion, as shown in Fig. 20(a)–(c). It is clearly seen that the dynamical forces for stick motion satisfy the criteria in the first equation of Eq. (38), and the vanishing of the stick motion satisfies the force requirement in Eq. (39) as well. The corresponding displacement, velocity, and forces responses for the periodic motion relative to $P_{2(01)^2}$ are presented in Fig. 20(d)–(f). The displacement, velocity and force responses for the periodic motion of P_{2101} are illustrated in Fig. 21. It is observed that only one stick motion exists in such a periodic motion. Once the stick motion vanishes, the non-stick motion will appear. For the complicated mapping $P_{(02)^2 01}$, several phase trajectories have been presented in Figs. 17 and 18. Herein, the further dynamical force relations with displacement and velocity are demonstrated in Fig. 22. The phase trajectory and forces responses of a periodic motion relative to $P_{(02)^2 01}$ become considerably complex compared to those simple stick and non-stick motions.

7. Conclusions

In this paper, the force criteria for the stick and non-stick motions in the harmonically forced, friction-induced oscillators are developed. The harmonically forced, linear oscillator with dry friction is investigated as an example for demonstration of the methodology. The stick and non-stick, periodic motions of such an oscillator is analytically predicted via appropriate mapping structures. The effects of the excitation and friction forces on the stick and non-stick motions are discussed and the corresponding parameter regions are obtained through the force criteria for stick and non-stick motions. The sliding and grazing bifurcations for this oscillator are also presented. However, a detailed investigation should be carried out further in sequel. The displacement, velocity and force responses for stick and non-stick, periodic motions are illustrated for a better understanding of the mechanism of stick and non-stick motions in the dry-friction oscillator. The methodology presented in this paper is applicable for numerical predictions of motions in nonlinear, non-smooth dynamical systems.

Appendix

Consider a linear oscillator in the domain Ω_j

$$\ddot{x}^{(j)} + 2d_j\dot{x}^{(j)} + c_i x^{(j)} = -b_j + A\cos\Omega t. \tag{A.1}$$

With the initial condition $(x_i, \dot{x}_i, t_i)$, solution for Eq. (A.1) in two regions $\Omega_j\,(j \in \{1,2\})$ are for *Case* I (*i.e.*, $d_j^2 > c_j$):

$$x^{(j)}(t) = C_1^{(j)}(x_i,\dot{x}_i,t_i)e^{\lambda_1^{(j)}(t-t_i)} + C_2^{(j)}(x_i,\dot{x}_i,t_i)e^{\lambda_2^{(j)}(t-t_i)} + A^{(j)}\cos\Omega t + B^{(j)}\sin\Omega t + C^{(j)}, \tag{A.2}$$

$$\dot{x}^{(j)}(t) = \lambda_1^{(j)}C_1^{(j)}(x_i,\dot{x}_i,t_i)e^{\lambda_1^{(j)}(t-t_i)} + \lambda_2^{(j)}C_2^{(j)}(x_i,\dot{x}_i,t_i)e^{\lambda_2^{(j)}(t-t_i)} - A^{(j)}\Omega\sin\Omega t + B^{(j)}\Omega\cos\Omega t, \tag{A.3}$$

$$\lambda_{1,2}^{(j)} = -d_j \pm \sqrt{d_j^2 - c_j}, \quad \omega_d^{(j)} = \sqrt{d_j^2 - c_j},$$

$$C_1^{(j)}(x_i, \dot{x}_i, t_i) = \frac{1}{2\omega_d^{(j)}}\left\{-\left[B^{(j)}\Omega + \left(d_j + \omega_d^{(j)}\right)A^{(j)}\right]\cos\Omega t_i + \left[A^{(j)}\Omega - \left(d_j + \omega_d^{(j)}\right)B^{(j)}\right]\sin\Omega t_i + \dot{x}_i - \left(d_j + \omega_d^{(j)}\right)\left(C^{(j)} - x_i\right)\right\},$$

$$C_2^{(j)}(x_i, \dot{x}_i, t_i) = \frac{1}{2\omega_d^{(j)}}\left\{\left[B^{(j)}\Omega - \left(\omega_d^{(j)} - d_j\right)A^{(j)}\right]\cos\Omega t_i - \left[\left(\omega_d^{(j)} - d_j\right)B^{(j)} + A^{(j)}\Omega\right]\sin\Omega t_i - \dot{x}_i + \left(\omega_d^{(j)} - d_j\right)\left(x_i - C^{(j)}\right)\right\}, \tag{A.4}$$

$$A^{(j)} = \frac{A_0\left(c_j - \Omega^2\right)}{\left(c_j - \Omega^2\right)^2 + \left(2d_j\Omega\right)^2}, \quad B^{(j)} = \frac{2d_j\Omega A_0}{\left(c_j - \Omega^2\right)^2 + \left(2d_j\Omega\right)^2}, \quad C^{(j)} = -\frac{b_j}{c_j}. \tag{A.5}$$

Case II (*i.e.*, $d_j^2 < c_j$):

$$x^{(j)}(t) = e^{-d_j(t-t_i)}\left[C_1^{(j)}(x_i, \dot{x}_i, t_i)\cos\omega_d^{(j)}(t - t_i) + C_1^{(j)}(x_i, \dot{x}_i, t_i)\sin\omega_d(t - t_i)\right] + A^{(j)}\cos\Omega t + B^{(j)}\sin\Omega t + C^{(j)}, \tag{A.6}$$

$$\dot{x}^{(j)}(t) = \left\{\left[\omega_d C_2^{(j)}(x_i, \dot{x}_i, t_i) - d_j C_1^{(j)}(x_i, \dot{x}_i, t_i)\right]\cos\omega_d(t - t_i) - \left[\omega_d C_1^{(j)}(x_i, t_i) + d_j C_2^{(j)}(x_i, \dot{x}_i, t_i)\right]\sin\omega_d(t - t_i)\right\}e^{-d_j(t-t_i)} - A^{(j)}\Omega\sin\Omega t + B^{(j)}\Omega\cos\Omega t, \tag{A.7}$$

$$\omega_d^{(j)} = \sqrt{c_j - d_j^2}, C_1^{(j)}(x_i, \dot{x}_i, t_i) = x_i - A^{(j)}\cos\Omega t_i - B^{(j)}\sin\Omega t_i - C^{(j)},$$

$$C_2^{(j)}(x_i, \dot{x}_i, t_i) = \frac{1}{\omega_d^{(j)}}\left[\dot{x}_i - \left(d_j A + B\Omega\right)\cos\Omega t_i - \left(d_j B^{(j)} - A^{(j)}\Omega\right)\sin\Omega t_i + d_j\left(x_i - C^{(j)}\right)\right]. \tag{A.8}$$

Case III (*i.e.*, $d_j^2 = c_j$):

$$x^{(j)}(t) = \left[C_1^{(j)}(x_i, \dot{x}_i, t_i) + C_2^{(j)}(x_i, \dot{x}_i, t_i) \times (t - t_i)\right]e^{\lambda_1^{(j)}(t-t_i)} + A^{(j)}\cos\Omega t + B^{(j)}\sin\Omega t + C^{(j)}, \tag{A.9}$$

$$\dot{x}^{(j)}(t) = \left[\lambda_1^{(j)}C_1^{(j)}(x_i, \dot{x}_i, t_i) + C_2^{(j)}(x_i, \dot{x}_i, t_i)\right]e^{\lambda_1^{(j)}(t-t_i)} + \lambda_1^{(j)}C_2^{(j)}(x_i, \dot{x}_i, t_i) \times (t - t_i)e^{\lambda_1^{(j)}(t-t_i)} - A^{(j)}\Omega\sin\Omega t + B^{(j)}\Omega\cos\Omega t, \tag{A.10}$$

$$\lambda_1^{(j)} = -2d_j, \quad C_1^{(j)}(x_i, \dot{x}_i, t_i) = x_i - A^{(j)}\cos\Omega t_i - B^{(j)}\sin\Omega t_i - C^{(j)},$$

$$C_2^{(j)}(x_i, \dot{x}_i, t_i) = \dot{x}_i + \left(A^{(j)}\Omega - d_j B^{(j)}\right)\sin\Omega t_i - \left(d_j A^{(j)} + B^{(j)}\Omega\right)\cos\Omega t_i - d_j\left(C^{(j)} - x_i\right). \tag{A.11}$$

References

[1] A.C.J. Luo, B.C. Gegg. On the mechanism of stick and non-stick periodic motion in a forced oscillator including dry-friction, *Proceeding of IMECE 2004*, 2004; ASME International Mechanical Engineering Congress & Exposition, November 13–19, 2004, Anaheim, California. IMECE2004-59218.

[2] J.P. Den Hartog, Forced vibrations with Coulomb and viscous damping, *Transactions of the American Society of Mechanical Engineers* 53 (1931) 107–115.

[3] E.S. Levitan, Forced oscillation of a spring-mass system having combined Coulomb and viscous damping, *Journal of the Acoustical Society of America* 32 (1960) 1265–1269.

[4] M.S. Hundal, Response of a base excited system with Coulomb and viscous friction, *Journal of Sound and Vibration* 64 (1979) 371–378.

[5] S.W. Shaw, On the dynamic response of a system with dry-friction, *Journal of Sound and Vibration* 108 (1986) 305–325.

[6] B.F. Feeny, A nonsmooth Coulomb friction oscillator, *Physics D* 59 (1992) 25–38.

[7] B.F. Feeny, F.C. Moon, Chaos in a forced dry-friction oscillator: experiments and numerical modeling, *Journal of Sound and Vibration* 170 (1994) 303–323.

[8] B.F. Feeny, The nonlinear dynamics of oscillators with stick–slip friction, in: A. Guran, F. Pfeiffer, K. Popp (Eds.), *Dynamics with Friction*, World Scientific, River Edge, 1996, pp. 36–92.

[9] N. Hinrichs, M. Oestreich, K. Popp, Dynamics of oscillators with impact and friction, *Chaos, Solitons and Fractals* 8 (4) (1997) 535–558.

[10] N. Hinrichs, M. Oestreich, K. Popp, On the modeling of friction oscillators, *Journal of Sound and Vibration* 216 (3) (1998) 435–459.

[11] S. Natsiavas, Stability of piecewise linear oscillators with viscous and dry friction dampping, *Journal of Sound and Vibration* 217 (1998) 507–522.

[12] S. Natsiavas, G. Verros, Dynamics of oscillators with strongly nonlinear asymmetric damping, *Nonlinear Dynamics* 20 (1999) 221–246.

[13] R.I. Leine, D.H. Van Campen, A. De Kraker, L. Van Den Steen, Stick–slip vibrations induced by alternate friction models, *Nonlinear Dynamics* 16 (1998) 41–54.

[14] L.N. Virgin, C.J. Begley, Grazing bifurcation and basins of attraction in an impact-friction oscillator, *Physica D* 130 (1999) 43–57.

[15] P.L. Ko, M.-C. Taponat, R. Pfaifer, Friction-induced vibration-with and without external disturbance, *Tribology International* 34 (2001) 7–24.

[16] U. Andreaus, P. Casini, Friction oscillator excited by moving base and colliding with a rigid or deformable obstacle, *International Journal of Non-Linear Mechanics* 37 (2002) 117–133.

[17] J.J. Thomsen, A. Fidlin, Analytical approximations for stick-slip vibration amplitudes, *International Journal of Non-Linear Mechanics* 38 (2003) 389–403.

[18] W.J. Kim, N.C. Perkins, Harmonic balance/Galerkin method for non-smooth dynamical system, *Journal of Sound and Vibration* 261 (2003) 213–224.

[19] V.N. Pilipchuk, C.A. Tan, Creep-slip capture as a possible source of squeal during decelerating sliding, *Nonlinear Dynamics* 35 (2004) 258–285.

[20] A.C.J. Luo, *Analytical Modeling of Bifurcations, Chaos and Fractals in Nonlinear Dynamics*. Ph.D. Dissertation, University of Manitoba, Winnipeg, Canada, 1995.

[21] R.P.S. Han, A.C.J. Luo, W. Deng, Chaotic motion of a horizontal impact pair, *Journal of Sound and Vibration* 181 (1995) 231–250.

[22] A.C.J. Luo, An unsymmetrical motion in a horizontal impact oscillator, *ASME Journal of Vibrations and Acoustics* 124 (2002) 420–426.

[23] S. Menon, A.C.J. Luo, An analytical prediction of the global period-1 motion in a periodically forced, piecewise linear system, *International Journal of Bifurcation and Chaos* (2003) in press.

[24] A.C.J. Luo, S. Menon, Global Chaos in a periodically forced, linear system with a dead-zone restoring force, *Chaos, Solitons and Fractals* 19 (2004) 1189–1199.

[25] A.C.J. Luo, The mapping dynamics of periodic motions for a three-piecewise linear system under a periodic excitation, *Journal of Sound and Vibration* 283 (2005) 723–748.
[26] F. Pfeiffer, Unsteady processes in machines, *Chaos* 4 (1994) 693–705.
[27] F. Pfeiffer, Chr. Glocker, *Multibody Dynamics with Unilateral Contacts*, Wiley Series in Nonlinear Science, New York, 1996.
[28] F. Pfeiffer, Unilateral multibody dynamics, *Meccanica* 34 (2000) 437–451.
[29] F. Pfeiffer, Applications of unilateral multibody dynamics, *Philosophical Transactions Royal Society of London A* 359 (2001) 2609–2628.
[30] A.F. Filippov, Differential equations with discontinuous right-hand side, *American Mathematical Society Translations, Series 2* 42 (1964) 199–231.
[31] A.F. Filippov, *Differential Equations with Discontinuous Righthand Sides*, Kluwer Academic Publishers, Dordrecht, 1988.
[32] A.C.J. Luo, A theory for non-smooth dynamical systems on connectable domains, *Communication in Nonlinear Science and Numerical Simulation* 10 (2005) 1–55.
[33] A.C.J. Luo, Imaginary, sink and source flows in the vicinity of the separatrix of non-smooth dynamic system, *Journal of Sound and Vibration* 28 (2005) 443–456.
[34] A.C.J. Luo, B.C. Gegg, (2005). Force product criteria of the sliding motions in a periodically forced, linear oscillator including dry friction, In: Proceedings of IDETC 2005, 2005 ASME International Design Engineering Conferences & Computer and Information Conferences in Engineering, September 24–28, 2005, Long Beach, CA. DETC2005-84147.
[35] A.C.J. Luo, B.C. Gegg, Grazing phenomena in a periodically forced, friction-induced, linear oscillator, *Communications in Nonlinear Science and Numerical Simulation* (2005) in press.
[36] A.C.J. Luo, On the symmetry of motions in non-smooth dynamical systems with two constraints, *Journal of Sound and Vibration* 273 (2004) 1118–1126.